Wnt5 controls splenic myelopoiesis and neutrophil functional ambivalency during DSS-induced colitis

Yi Luan[1,10], **Jiajia Hu**[1,10], **Qijun Wang**[1,10], **Xujun Wang**[8,9,10], **Wenxue Li**[5,10], **Rihao Qu**[2,3,4], **Chuan Yang**[1], **Barani Kumar Rajendran**[1], **Hongyue Zhou**[1], **Peng Liu**[1], **Ningning Zhang**[8,9], **Yu Shi**[6], **Yansheng Liu**[5,7,*], **Wenwen Tang**[1,*], **Jun Lu**[8,9,*], **Dianqing Wu**[1,11,*]

[1]Department of Pharmacology, Vascular Biology and Therapeutic Program, Yale School of Medicine, New Haven, CT 06519, USA

[2]Department of Immunobiology, Yale University School of Medicine, New Haven, CT 06520, USA

[3]Program of Computational Biology and Bioinformatics, Yale University, New Haven, CT 06520, USA

[4]Department of Pathology, Yale University School of Medicine, New Haven, CT 06510, USA

[5]Yale Cancer Biology Institute, West Haven, CT 06516, USA

[6]School of Management, Yale University, New Haven, CT 06511, USA

[7]Department of Pharmacology, Yale University School of Medicine, New Haven, CT 06510, USA

[8]Department of Genetics, Yale University School of Medicine, New Haven, CT 06510, USA

[9]Yale Stem Cell Center, Yale University, New Haven, CT 06520, USA

[10]These authors contributed equally

[11]Lead contact

SUMMARY

Neutrophils are important innate immune cells with plasticity, heterogenicity, and functional ambivalency. While bone marrow is often regarded as the primary source of neutrophil production, the roles of extramedullary production in regulating neutrophil plasticity and heterogenicity in autoimmune diseases remain poorly understood. Here, we report that the lack of wingless-type MMTV integration site family member 5 (WNT5) unleashes anti-inflammatory protection against colitis in mice, accompanied by reduced colonic CD8^{+} T cell activation and enhanced splenic extramedullary myelopoiesis. In addition, colitis upregulates WNT5 expression in splenic stromal

*Correspondence: yansheng.liu@yale.edu (Y.L.), wenwen.tang@yale.edu (W.T.), jun.lu@yale.edu (J.L.), dianqing.wu@yale.edu (D.W.).

AUTHOR CONTRIBUTIONS

DECLARATION OF INTERESTS

The authors declare no competing interests.

SUPPLEMENTAL INFORMATION

Supplemental information can be found online at https://doi.org/10.1016/j.celrep.2024.113934.

cells. The ablation of WNT5 leads to increased splenic production of hematopoietic niche factors, as well as elevated numbers of splenic neutrophils with heightened CD8^{+} T cell suppressive capability, in part due to elevated CD101 expression and attenuated pro-inflammatory activities. Thus, our study reveals a mechanism by which neutrophil plasticity and heterogenicity are regulated in colitis through WNT5 and highlights the role of splenic neutrophil production in shaping inflammatory outcomes.

In brief

Luan et al. report that the absence of WNT5 proteins in mice increases, through splenic granulopoiesis, the production of CD101-high hyper-immunosuppressive and hypo-inflammatory neutrophils. These neutrophils protect the mice from DSS-induced colitis.

Graphical abstract
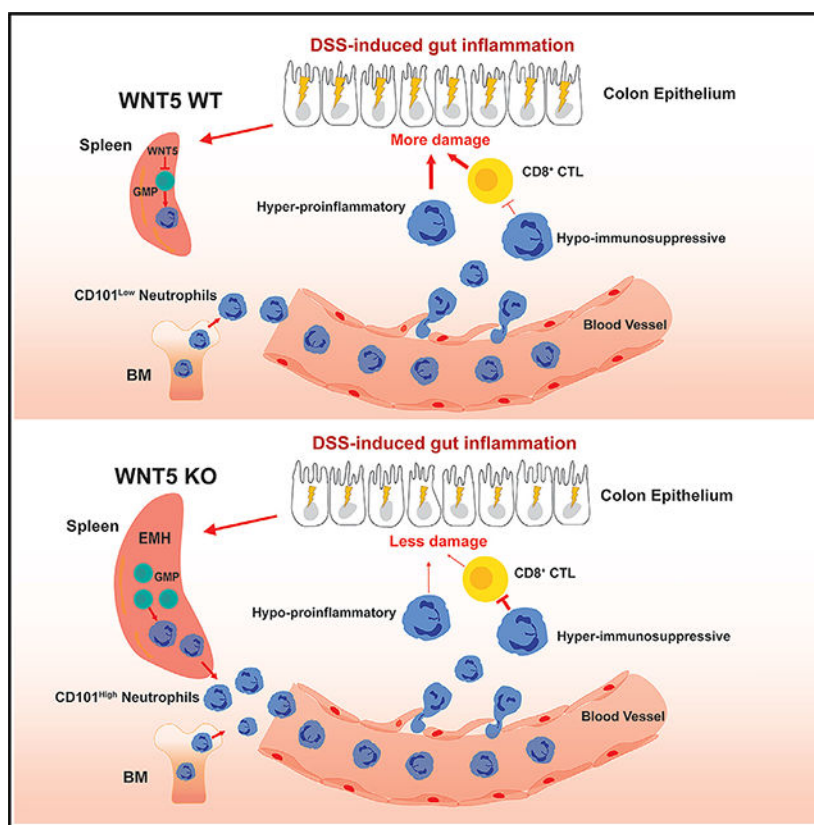
INTRODUCTION

Neutrophils are the most abundant leukocytes in human blood and the first to be recruited to the sites of inflammation.[1–9] They play ambivalent roles in organismal well-being. While they are important for host defense against microbial infections, the products released by neutrophils upon activation can cause tissue damage. In addition, their immunosuppressive activity can be beneficial to some inflammation diseases including inflammatory bowel disease (IBD), although this activity can also promote tumor formation.[10–13] The

effects of neutrophils on disease outcomes are the summation of their detrimental vs. beneficial effects. This functional ambivalency of neutrophils is at least in part due to neutrophil plasticity and heterogenicity.[1,2,6,14,15] Investigations on neutrophil plasticity and heterogenicity have been largely carried out in the context of tumor immunity.[16–18] However, neutrophil plasticity and the functional roles of diverse neutrophil subpopulations in the context of non-tumor inflammation have been poorly investigated and understood.

Ulcerative colitis and Crohn's disease, collectively known as IBD, are autoimmune gastrointestinal diseases. IBD affects millions of people worldwide, particularly in developed countries, and its etiology seems to be complex and attributed to a combination of environmental factors, defective immune responses, intestinal microbiota, and genetic susceptibility.[19–21] The immune responses are important for the pathogenesis of the disease. Although CD4$^+$ T cells play key roles in the initiation and progression of the disease, the conventional cytotoxic CD8$^+$ T cells, which have high granzyme B (GZMB) expression, primarily associate with mucosal damage and exacerbate pathogenesis during colitis.[22–28] However, in different experimental models, subsets of CD8$^+$ T cells that exhibit suppressive or regulatory roles within the immune system were also described. These CD8$^+$ T cells have low GZMB expression but express anti-inflammatory cytokines like interleukin-10 and transforming growth factor β (TGF-β) and inhibitory receptors. These regulatory CD8$^+$ T cells contribute to immune modulation and suppress or eliminate activated CD4 T cells.[29–31] The neutrophil also plays an important role in human and mouse models of IBD.[10,32,33] However, how neutrophils impact IBD is not well understood.

Wingless-type MMTV integration site family member 5 (WNT5) consists of two members, WNT5A and WNT5B, which share 90% amino acid sequence identity.[34] These WNT5 proteins are involved in diverse physiological and pathological processes, including stem cell self-renewal, cell proliferation, differentiation, migration, adhesion, and polarity.[35–37] *Wnt5a* gene knockout (KO) causes embryonic lethality with significant developmental defects in mice, whereas *Wnt5b* KO mice do not show strong phenotypes. While evidence indicates that WNT5A and WNT5B may have redundant roles in some developmental and physiological processes, including governing the break of left-right symmetry and neuronal specification, evidence also exists for them having distinct functions.[36–40] The WNT5A protein has been linked to intestinal physiology and pathophysiology through multiple regulatory mechanisms. It is involved in crypt regeneration to re-establish homeostasis after intestinal injury[41] and may promote the ability of intestinal dendritic cells (DCs) to facilitate the differentiation of naive CD4$^+$ T cells into interferon-γ-producing CD4$^+$ T helper type 1 (Th1) cells in a colitis model.[42] It is not known if WNT5B plays a role in, or if WNT5A and WNT5B have a redundant role in, the regulation of intestinal biology and inflammation.

In this article, we found that double KO of WNT5A and WNT5B (WNT5 DKO) protected mice from dextran sulfate sodium (DSS)-induced colitis. In addition, we found that the deficiency of WNT5 led to the production of neutrophils from the spleen with heightened suppressive activity toward CD8$^+$ T cells and reduced production of reactive oxygen species (ROS) and neutrophil extracellular traps (NETs) upon colitis induction. Importantly, these neutrophils from the spleen were required for colitis protection of these *Wnt5* DKO mice.

Thus, the study revealed an unexpected role of WNT5 in the regulation of neutrophil plasticity and the importance of neutrophil plasticity in experimental colitis.

RESULTS

Wnt5 DKO mice are less susceptible to DSS-induced colitis

The wild-type (WT) mice, WNT5A and 5B DKO (*Rosa26-Cre^{ERT2}Wnt5a$^{flox/flox}$Wnt5b$^{-/-}$*, referred as *Wnt5* DKO after the administration of tamoxifen) mice, and mice with various intermediate genotypes, including heterozygous WNT5B KO mice (*Wnt5b$^{+/-}$*), WNT5B KO mice (*Wnt5b$^{-/-}$*), WNT5A KO/WNT5B heterozygous mice (*Rosa26-Cre^{ERT2}Wnt5a$^{flox/flox}$Wnt5b$^{+/-}$*, referred to as *Wnt5a$^{-/-}$Wnt5b$^{+/-}$* after the administration of tamoxifen) were subjected to DSS-induced colon inflammation (Figure S1A). The DKO mice showed less weight loss than the WT control mice, whereas no significant differences were observed in weight loss among WT mice and mice with intermediate genotypes (Figure 1A). The other colitis phenotypes, including the disease activity index and colon length shortening, were also significantly milder in the *Wnt5* DKO mice than those of WT mice and littermates with other intermediate genotypes, while there were no significant differences among WT mice and the mice with intermediate genotypes (Figures 1B, 1C, and S1B). No difference was observed in colon length before DSS treatment (Figure S1C). Although WNT5 loss did not alter colon histological structure before DSS treatment, colon tissues in the *Wnt5* DKO mice showed less damaged glands, goblet cells, mucosal architecture, and villa structures than those in the control mice after DSS treatment (Figures 1D, 1E, S1D, and S1E). These results together suggest that mice lacking both WNT5A and WNT5B are less susceptible to DSS-induced colitis. As the *Wnt5* DKO mice showed much stronger resistance to colitis phenotypes than any of the intermediate genotypes, WNT5A and WNT5B are likely functionally redundant in colitis regulation.

Wnt5 DKO mice increase myeloid cell abundance and suppress cytotoxic CD8$^+$ T cells in DSS-treated colons

Immune cells are known to play a crucial role in the pathogenesis of colitis. We therefore examined whether loss of the WNT5 protein altered immune cell composition during colitis (Figures S2A–S2C). Since WT mice and *Wnt5b$^{+/-}$* mice showed similar colitis phenotypes, either WT or *Wnt5b$^{+/-}$* littermates of the *Wnt5* DKO mice were used as the controls. The percentages and total numbers of neutrophils and monocytes significantly increased in the colon intraepithelial layer and lamina propria of the *Wnt5* DKO mice, while macrophages and DCs remained unchanged (Figures 2A–2D and S2D–S2G). The percentages and numbers of CD4$^+$ T cells, CD8$^+$ T cells, regulatory T cells, Th17 cells, and B lymphocytes were largely unaltered in the colons (Figures 2E, 2F, and S2H–S2Q). However, *Wnt5* DKO mice significantly decreased GZMB expression in colonic CD8$^+$ T cells (Figures 2G and 2H).

Colitic *Wnt5* DKO mice develop splenomegaly

We also noticed that DSS-treated *Wnt5* DKO mice had significantly enlarged spleens over the control mice (Figures 3A and S3A). Such a difference was not observed before DSS treatment (Figure S3B). The *Wnt5* DKO spleens had significantly increased percentages

and numbers of neutrophils, monocytes, erythrocytes, and megakaryocytes over spleens of control mice (Figures 3B–3E and S3C–S3E). Splenic macrophages showed trends of increases in the *Wnt5* DKO mice in both percentage and cell number, whereas DCs, CD4+ T cells, CD8+ T cells, and B cells were largely unaltered by WNT5 deficiency (Figures S3F–S3J).

The *Wnt5* DKO mice also had increased percentages of neutrophils in the blood and mesenteric lymph node (MLN) (Figures 3F and 3G) but not in the bone marrow (Figure S3K). In addition, the *Wnt5* DKO mice had increased percentages of monocytes and macrophages in the MLN (Figure 3G) but not in the blood or bone marrow (Figures 3F–3S3K). The percentages of CD4+, CD8+ T cells, or B cells in the blood, MLN, or bone marrow of the *Wnt5* DKO mice did not show changes from those of the control mice (Figures S3L–S3N). Thus, upon DSS treatment, loss of WNT5 resulted in splenomegaly and a more pronounced expansion of myeloid cells in the spleen, lymph nodes, and peripheral blood compared to the control mice, without obvious effects on other leukocytes.

WNT5 deficiency enhances splenic EMH and myelopoiesis upon colitis induction

Splenomegaly is often the result of splenic extramedullary hematopoiesis (EMH). To investigate the hematopoiesis in the spleen, we examined hematopoietic stem and progenitor cells in the spleen. Indeed, the lack of WNT5 significantly increased the percentage and number of splenic stem cells (defined as Lineage−c-Kit+Sca-1+ [LSK] cells) and progenitor cells (defined as Lineage−Sca-1−c-Kit+ [LK] cells) (Figures 4A, 4B, and S4A) as well as granulocyte and monocyte progenitors (GMPs) and megakaryocytes progenitor cells (MKPs) (Figures 4C and 4D). By contrast, WNT5 deficiency reduced LSK cells, LK cells, GMPs, and MKPs in the bone marrow (Figures S4B and S4C).

We next sorted splenic CD45+ cells from DSS-treated WT mice and *Wnt5* DKO mice and carried out single-cell RNA sequencing (scRNA-seq). Unsupervised clustering identified 16 cell clusters that belonged to 8 major cell populations based on lineage marker expression (Figures 4E, S4D, and S4E; Table S1). The percentage of myeloid cells, including neutrophils, monocytes, and their progenitor cells, markedly expanded in the DKO spleens over the WT spleens (Figure 4F). We next focused on cell clusters expressing neutrophil markers *Ly6G*, *Cxcr2*, and/or *S100a8*, which were partitioned into four subclusters, N0–N3 (Figure 4G). The N0–N3 subclusters represented the neutrophil differentiation trajectory based on the markers of bone marrow neutrophil development.[43] The N0 subcluster expressed progenitor RNA markers (*Elane, Mpo, Prtn3*), cell cycle and proliferation markers (*Mki67* and *Cdc20*), and higher ribosomal protein genes, therefore representing neutrophil progenitors. Expression of these N0 marker genes started to wane in the N1 subcluster, with further declines in the N2 and N3 subclusters. In contrast, mature neutrophil marker genes such as *Cxcr2* and *Ccl6* started to express in the N2 subcluster and were further elevated in the N3 subcluster (Figure S4F; Table S2). Compared to the WT spleen neutrophils, the *Wnt5* DKO spleen neutrophils underwent a similar developmental trajectory but with substantially larger fractions of the continuum from N0 to N2 subpopulations and a drastically reduced N3 subpopulation (Figure 4H). These results together suggest that splenic granulopoiesis of both *Wnt5* DKO and WT colitic mice closely resembles bone marrow granulopoiesis.

The apparent enrichment of more immature neutrophils in the spleens of DSS-treated *Wnt5* DKO mice suggests either retarded neutrophil maturation or accelerated release of mature neutrophils in these spleens compared to the control spleens.

Splenic-stromal-cell-derived WNT5 is the potential regulator of EMH in the spleen

Real-time qPCR and scRNA-seq analysis of spleen cells determined that *Wnt5* expression was barely detected in CD45^{+} spleen cells but restricted to *Pdgfra*^{+} and *Pdgfrβ*^{+} stromal cells, including *Wt1*^{+} fibroblast and *Myh11*^{+} smooth muscle cells (Figures 4I and S4G). DSS treatment significantly increased the *Wnt5* expression in the splenic *Pdgfra*[+] and *Pdgfrβ*^{+} stromal cells (Figure 4I). Splenic stromal cells produce various niche factors that are important for EMH.[44,45] Indeed, *Wnt5* DKO mice increased the expression of *Cxcl12*, *Tgfb1*, and *Jag1* in the *Pdgfra*[+] and *Pdgfrβ*^{+} stromal cells (Figure 4J). CXCL12 is a key niche factor for splenic EMH.[46] The increase in the *Cxcl12* mRNA in the spleen stromal cells of *Wnt5* DKO mice was further confirmed by RT-qPCR (Figure 4K). Thus, splenic-stromal-cell-derived WNT5 may regulate splenic EMH via the regulation of the expression of hematopoietic niche factors including CXCL12.

Colitis-protection phenotypes of *Wnt5* DKO mice depend on splenic neutrophils

To examine if neutrophils might be responsible for the colitis-protection phenotypes, we performed neutrophil depletion using an anti-Ly6G antibody (Figure S5A), which effectively depleted neutrophils in the spleen, bone marrow, peripheral blood, and colon (Figure S5B). Depletion of neutrophils markedly exacerbated colitis phenotypes in the *Wnt5* DKO mice and also significantly, but to a lesser extent, aggravated the colitis phenotypes in the control mice (Figures 5A–5C). Importantly, neutrophil depletion abrogated the differences in colitic phenotypes between the *Wnt5* DKO mice and control mice (Figures 5A–5C). However, neutrophil depletion did not appear to affect enlarged spleens. This might be because neutrophil depletion did not affect the expansion of monocytes and erythroid cells in the DKO spleens (Figures S5C–S5E). While neutrophil depletion did not alter colonic CD8^{+} T cells and other lymphocytes (Figures S5F–S5H), it increased colonic GZMB^{+}CD8^{+} T cells in both control and DKO mice, and importantly, it abrogated the differences in GMZB^{+}CD8^{+} T cells between the DKO mice and control mice (Figure 5D). These data suggest that neutrophils play a moderate role in the resistance to DSS-induced colitis in the WT mice and that this role of neutrophils is greatly amplified in the absence of WNT5.

We next tested the idea that the increase in splenic granulopoiesis is responsible for the colitis phenotypes of *Wnt5* DKO mice by performing splenectomy right before DSS treatment. Splenectomy abrogated the differences in the colitis phenotypes between *Wnt5* DKO mice and control mice by exacerbating colitis phenotypes in *Wnt5* DKO mice (Figures 5E–5H, S5I, and S5J). Splenectomy also increased colonic CD8^{+} T cell GZMB expression in the *Wnt5* DKO mice without significantly affecting that of control mice (Figures 5E–5H, S5I, and S5J). These data together provide strong support for the conclusion that neutrophils produced by the spleen are largely responsible for the colitis phenotypes of *Wnt5* DKO mice.

Colitic *Wnt5* DKO mice produce CD101-high hyper-immunosuppressive neutrophils from the spleen

To understand how spleen-derived neutrophils in *Wnt5* DKO mice control colonic inflammation, we performed scRNA-seq and proteomic analysis of Ly6G$^+$ neutrophils from the blood of DSS-treated *Wnt5* DKO mice and control mice, designated as DKO-DSS and WT-DSS, respectively. Differential gene expression (DEG) analysis of the scRNA-seq data identified 1,472 upregulated and 394 downregulated genes in circulating neutrophils when comparing DKO-DSS to the WT-DSS mice (Table S3). The proteomic analysis revealed 319 proteins significantly upregulated and 408 downregulated (Table S4). Among these proteins, 77 and 52 were also found to be upregulated and downregulated in the transcriptomic analysis, respectively (Figure 6A; Table S5). The pathway and Gene Ontology analyses indicated that the overlapping genes were significantly enriched in pathways related to neutrophil functions including the ROS metabolic process and T cell activation activities and pathways (Figures S6A–S6C; Table S6). Among the overlapping genes, the most differentially regulated one is CD101, whose expression correlates to T cell suppression and colitis.[47,48]

While there was no difference in cell surface CD101 expression of blood neutrophils between WT mice and DKO mice without DSS treatment (Figure 6B), DSS treatment led to a marked suppression of CD101 expression of WT blood neutrophils (Figure 6B) compared to non-DSS treatment samples. *Wnt5* DKO mice largely prevented CD101 downregulation after DSS treatment (Figure 6B). Importantly, when these blood neutrophils were isolated by cell sorting and cocultured with splenic CD8$^+$ T cells, the suppressive activities of these blood neutrophils on CD8$^+$ T cells largely correlated with neutrophil CD101 expression (Figures 6C–6E, S6D, and S6E). Additionally, the CD101-high neutrophils showed greater immunosuppressive activities than the CD101-low cells sorted from the same blood cells of DKO-DSS mice (Figures 6F–6I). Moreover, the CD101-low cells showed comparable immunosuppressive activities to the blood neutrophils from WT-DSS mice (Figures 6G–6I), whose CD101 expression was similar to that of CD101-low cells (Figure 6B). Therefore, the enhanced immunosuppressive activity of these CD101-high neutrophils may help to explain the strong suppression of CD8$^+$ T cells observed in the DKO-DSS mice.

To test whether the spleen is the source of these circulating CD101-high neutrophils in the DKO-DSS mice, we performed a cell tracing experiment by injecting carboxyfluorescein succinimidyl ester (CSFE) dye into the bone marrow and the Far-Red dichloro dimethyl acridin one succinimidyl ester (DDAO-SE) dye into the spleen of WT-DSS and DKO-DSS mice, respectively (Figure S6F). Fractions of neutrophils stained either with CSFE or Far-Red were detected 2 h later in the blood, but those stained with both dyes were extremely rare (Figures 6J and S6G), suggesting that the dyes only stained cells within their tissue compartments where they were injected. Thus, CSFE$^+$ cells in the blood were primarily released from the bone marrow, whereas Far-Red$^+$ cells were primarily from the spleen. The blood Far-Red$^+$ neutrophils, which were produced from spleens, showed high CD101 expression regardless of their WT or DKO origin, whereas the blood CSFE$^+$ neutrophils showed low CD101 expression (Figure 6J). Concordantly, Far-Red-stained neutrophils in the spleen had high CD101 expression, whereas CSFE-stained neutrophils in the bone marrow

had low CD101 expression (Figure S6G). Moreover, more spleen-originated neutrophils infiltrated into inflamed colon tissues of the *Wnt5* DKO mice than bone-marrow-originated neutrophils (Figure S6H). Thus, these results, together with splenectomy reducing CD101 expression in the DKO-DSS blood neutrophils (Figure S6I), indicate that the CD101-high neutrophils are predominately released from the spleens and that spleen-originated neutrophils may have stronger infiltration ability than bone-marrow-originated ones into the inflamed colon.

CD101 directly contributes to CD8^{+} T cell suppression

We next investigated whether CD101 merely served as a marker for the subpopulation of neutrophils with heightened immunosuppressive activity or also directly contributed to T cell suppression. The Ly6G^{+} neutrophils sorted from the DKO-DSS spleens were transiently transfected with the SMARTpool ON-TARGETplus small interfering RNAs specific for *Cd101*. The knockdown of CD101 was confirmed by flow cytometry (Figure 6K). Importantly, CD101 knockdown significantly reduced the suppressive activities of the neutrophils on CD8^{+} T cells (Figures 6L–6N). Moreover, recombinant CD101 also strongly inhibited CD8^{+} T cell activation (Figure S6J). Therefore, the CD101 molecule itself directly contributes to CD8^{+} T cell suppression.

Transcriptomic profiles of blood neutrophils inform the functions of colon neutrophils

Flow cytometry analysis showed that colon-infiltrated neutrophils in DKO-DSS mice had higher levels of CD101 (Figure 7A) and lower citrullinated histone (NET formation marker) and ROS than those of WT-DSS mice (Figures 7B and S7A). However, the DEG analysis of scRNA-seq datasets of colon-infiltrated Ly6G^{+} neutrophils between DKO-DSS and WT-DSS mice identified only 30 upregulated and 22 downregulated genes (Table S7). Not only was the *Cd101* RNA not among the DEGs, but also the pathway and Gene Ontology analyses of these DEGs did not implicate functional differences in ROS production or NET formation, whereas the analyses of DEGs of blood neutrophil did (Figures S6B and S6C; Tables S6 and S7). To understand why, we further analyzed the scRNA-seq data of colon and blood neutrophils from DKO-DSS and WT-DSS mice, together with published scRNA-seq data of neutrophils from untreated WT mice, peritonitis, and tumor-bearing mouse models.[14,49–51]

Unsupervised clustering of these neutrophils revealed 7 major clusters (Figures 7C and S7B; Table S8). Blood neutrophils were primarily distributed in clusters 1, 2, 3, and 5 (Figures 7C–7E). The WT-DSS blood neutrophils were dominated by cluster 3 (~50%), with fewer cells in clusters 1 (17%), 2 (14%), and 5 (3%) (Figures 7C–7E). By contrast, the DKO-DSS blood neutrophils showed a substantial reduction in cluster 3 (18%) and a more balanced distribution among clusters 1 (34%), 2 (22%), 3 (18%), and 5 (17%) (Figures 7C–7E). In addition, the DKO-DSS blood neutrophils more closely resembled untreated WT ones that had a smaller fraction of cells in cluster 3 (8%) and occupied primarily clusters 2 (50%) with fewer cells also in clusters 1 (21%) and 5 (8%) (Figures 7C–7E). The gene expression profiles of the blood neutrophils from the peritonitis model and tumor-bearing mice appeared to be in between those of WT-DSS and DKO-DSS blood neutrophils (Figures 7C–7E). In contrast to blood neutrophils, tissue neutrophils were predominantly populated

in cluster 0, regardless of the models or conditions (Figures 7C–7E). Consistent with a low number of DEGs between WT-DSS and DKO-DSS colon neutrophils, these colon neutrophils, largely occupying cluster 0, showed similar uniform manifold approximation and projection patterns (Figures 7C–7E). These results suggest that different mouse models or inflammation conditions are associated with more diverse gene expression profiles of circulating neutrophils than those of the tissue neutrophils.

We next compared the gene expression signature scores for ROS and NETs.[14,52] WT-DSS blood neutrophils were dominant in cluster 3, which showed markedly higher scores of ROS and NETs than the other blood neutrophil clusters (1, 2, and 5), which were predominantly occupied by the DKO-DSS neutrophils (Figure 7F). Both WT-DSS and DKO-DSS colon neutrophils were populated in cluster 0 and thus have the same ROS and NET scores (Figure 7F). However, given that WT and DKO colon neutrophils showed different ROS and NET production experimentally (Figure 7B), the blood neutrophil gene expression functional scores aligned better with the experimental functional outcomes than the gene expression scores of colon neutrophils and may be better indicators of functional impacts of neutrophils.

We also compared the tumor myeloid-derived suppressor cell (MDSC) score based on previously published gene signatures.[49] Concordantly, clusters 1 and 5, where the tumor blood neutrophils largely populated, showed higher MDSC scores than the other major clusters (Figure 7G). Consistent with the low immunosuppressive activity of WT-DSS blood neutrophils (Figure 6), cluster 3, where WT-DSS blood neutrophils occupied, had lower MDSC scores than clusters 1 and 5. Thus, in addition to CD101, which is important for immunosuppression in the context of colitis, some of the MDSC immunosuppressive mechanisms may also be involved in colitis. While the gene expression scores for ROS, NETs, and MDSCs (Figures 7F and 7G) and the expression levels of *Cd101* and *Ly6g* RNA (Figure 7H) of colon neutrophils were on the low side compared to those of blood neutrophils, the chemotaxis score of the colon neutrophils is higher (Figure 7I). In addition, RNA expression of genes related to pro-apoptosis (*Bcl2l11*, *Ctsb*, and *Gadd45b*), neutrophil/ monocyte recruitment, and macrophage function (*Cxcl3, Cxcl2 Ccl3*, *Ccl4*, and *Csf1*) was higher in cluster 0 than the blood neutrophil clusters (Figures 7H and S7B; full gene names of all gene symbols are listed in Table S9). These results suggest that the transcriptional activity of some neutrophil-function-related genes subsided once the neutrophils reached the colon, where the neutrophils progress into a different transcriptional state that seems to favor inflammation amplification and/or resolution. As protein content changes may lag RNA content changes, the differences in RNA expression of blood neutrophils may transit to protein content differences and subsequent functional differences in colon neutrophils. The better alignment of blood neutrophil CD101 RNA expression with CD8+ T cell suppression in the colon and the better alignment of ROS and NET scores of blood neutrophils with ROS production and NET content in colon neutrophils indicate that the RNA expression profiles of blood neutrophils are informative of the functional outcomes of colon neutrophils. Together with the observation that colon neutrophils expressed the highest CD101 among all of CD45+ leukocytes in the inflamed colons (Figure S7C), we conclude that these hyper-immunosuppressive and hypo-inflammatory characteristics of DKO-DSS neutrophils shape an anti-inflammatory environment in the inflamed colon (Figure S7D).

DISCUSSION

In this study, we uncovered that WNT5A and WNT5B constituted a negative feedback mechanism for controlling splenic EMH and granulopoiesis during colitis. Their deficiency increased the production of CD101-high hyper-immunosuppressive and hypo-inflammatory neutrophils from the spleen to protect against colitic injury. These results not only support the role of spleen-derived neutrophils in providing anti-inflammatory protection against DSS-induced colitis but also suggest that, under autoimmune conditions, myeloid progenitors in the spleen and bone marrow are pre-programmed to give rise to neutrophils with different anti-inflammatory capacities.

Neutrophils are known to play complex roles in inflammation. Our present study revealed that the complex roles of neutrophils in IBD were at least in part due to their sources. In the context of gut inflammation, the spleen produces CD101-high neutrophils that are hyper-immunosuppressive and hypo-inflammatory, in contrast to those from the bone marrow, and exert more protective than tissue-damaging effects in the colon. We also revealed that WNT5 proteins were the important negative regulators of splenic granulopoiesis as well as EMH. EMH can be triggered by various conditions including chronic inflammatory conditions such as human and mouse IBD.[53–57] However, little is known about how EMH is regulated or what actual roles EMH plays in various diseases. Given that WNT5 expression was upregulated by colitis, it constitutes a negative feedback mechanism for the regulation of splenic EMH, which often skews toward myelopoiesis and, hence, granulopoiesis. WNT5 likely regulates EMH via suppression of the expression of hematopoietic niche factors including CXCL12 in splenic stromal cells.

Current knowledge on the regulation of neutrophil heterogeneity and functional diversity has largely come from studies of neutrophils or MDSCs in the context of tumor immunity. Spleens were also shown as a source of MDSCs in tumor-bearing mice,[58,59] but neutrophils undergo further remodeling or reprogramming once they reach the tumors, leading to additional diversity.[1,2,6,16–18,49,50,58,60–66] Colon-infiltrated neutrophils appeared to be less diverse in their RNA expression profiles than tumor-infiltrated neutrophils or even their precursors, the blood neutrophils (Figures 7C and 7D). ROS is a key mediator for the immunosuppressive action of MDSCs in the context of tumor immunity.[60] However, the blood DKO-DSS neutrophils had lower ROS gene expression signature scores and the colon DKO-DSS neutrophils had less ROS activity than the WT-DSS counterparts. Thus, ROS may not be responsible for the increased immunosuppression of DKO-DSS neutrophils over WT-DSS ones. Instead, we demonstrated that CD101 may contribute to enhanced immunosuppression of these cells. This is consistent with the observation that the loss of CD101 expression in mouse myeloid cells is associated with exacerbated colitis.[47] The inverse correlation of CD101 expression with the severity of the IBD in humans[47,48] highlights the relevance of our findings to human IBD pathogenesis. Future studies are needed to further determine the contribution of neutrophil-mediated cytotoxic CD8+ T cell suppression to DKO mice colitis phenotypes relative to other mechanisms, including neutrophil ROS and NET production, as well as possible effects of DSS-DKO neutrophils on other immune cells.

Limitations of the study

While our study effectively demonstrates that the loss of WNT5 protects mice against DSS-induced colitis by enhanced splenic granulopoiesis, it is essential to acknowledge that the beneficial impact of WNT5 deficiency on colitis onset may involve additional mechanisms. This consideration arises from the fact that WNT5 is expressed not only in splenic cells but also in various other cell types within the colon. Our findings highlight the reduction in colon inflammation achieved through the generation of neutrophils from *Wnt5* DKO spleens during colitis. These neutrophils exhibit the capability to suppress cytotoxic CD8$^+$ T cells and reduced ability to produce ROS and NETs. However, due to the intricate nature of colitis pathology and the complexity of the colon microenvironment, it remains unclear which specific aspects play a more predominant role in mediating the observed protective effects and whether other immune cells also play secondary roles. In addition, this study focuses on the acute injury phase of colitis. The WNT5 proteins may have additional roles in the recovery phase of the disease.

STAR★METHODS

RESOURCE AVAILABILITY

Lead contact—Further information and requests for resources and reagents should be directed to and will be fulfilled by the lead contact, Dianqing Wu (dianqing.wu@yale.edu).

Materials availability—This study did not generate new unique reagents.

Data and code availability

- Proteomics data have been deposited at ProteomeXchange database (ProteomeXchange: PXD048613). To review the dataset please go to https://www.ebi.ac.uk/pride/login and use the following login details: Username: reviewer_pxd048613@ebi.ac.uk; Password: wZ1f6cRb). The data of Single-cell RNA-seq has been submitted to the NCBI GEO: GSE255409. They are publicly available as of the date of publication.

- This paper does not report the original code.

- Any additional information required to reanalyze the data reported in this paper is available from the lead contact upon request.

EXPERIMENTAL MODEL AND STUDY PARTICIPANT DETAILS

Animal— *Wnt5a$^{flox/flox}$, Wnt5b$^{-/-}$*, and *Rosa26Cre^{ERT2}* mice were purchased from Jackson Laboratory. The *Wnt5* DKO (Genotype: *Rosa26-Cre^{ERT2}Wnt5a$^{flox/flox}$Wnt5b$^{-/-}$*) mice were generated by crossing *Rosa26-Cre^{ERT2}* mice with *Wnt5a$^{flox/flox}$* and *Wnt5b$^{-/-}$* mice. All mice had been backcrossed into the C57Bl background prior to the intercrosses. All mice were age- (8 weeks old at the start of experiments) and sex-matched (both male and female mice were used). Littermate controls were used where appropriate. Mice were maintained in specific pathogen-free animal facilities at Yale University. The mice were housed under 12-h light/dark cycles with free access to food and sterile water. All experiments were performed

in accordance with guidelines from the Institutional Animal Care and Use Committee at Yale University.

METHOD DETAILS

DSS-induced colitis—To generate the *Wnt5* DKO mice, 100 mg/kg mouse body weight Tamoxifen (Sigma T-5648) dissolved in corn oil (Sigma C-8267) was delivered to mice at 8 weeks old through i.p injection. To induce colitis, 2% DSS (MP Biomedicals) was then delivered to mice in drinking water for 7 days at 13 weeks old. Body weight loss as a clinical sign of colitis was recorded daily. The disease activity index including the presence of blood in stool, stool consistency, and rectal prolapse was calculated daily as has been previously described.[67] Colonic lengths were measured immediately after colons were excised.

Colon histology—H&E staining of colon tissues was performed at the Comparative Pathology Research core at Yale School of Medicine. Briefly, colons were excised, flushed with PBS, opened longitudinally, arranged in swiss rolls, and fixed in 4% buffered formalin overnight. They were then embedded in paraffin, sectioned (5 μm), and stained with hematoxylin/eosin (H&E) according to standardized protocols. Slides were imaged using an Aperio eSlide Scanner (Leica Biosystems).

Neutrophil depletion *in vivo*—Depletion of $Ly6G^+$ neutrophils was performed by i.p. injection of the anti-Ly6G mAb (1A8, BioXCell BE0075) at a dose of 500 μg in 200 μL PBS per mouse. Anti-Ly6G mAb was delivered every day starting from day −1 to day 6 of DSS treatment. Control mice received corresponding isotype mAb (BioXCell BE0089).

In vitro T cell suppression assay—$CD8^+$ T cell preparation: Splenocytes were freshly isolated from mice. Red blood cells were lysed using Red Blood Cell lysis buffer (RBC lysis buffer, R7757, Sigma) before being magnetically sorted using the $CD8^+$ T cell isolation kit (Catalog # 130-096-543, Miltenyi Biotec). Neutrophil preparation: Splenocytes and blood cells were freshly isolated from mice. Red blood cells were lysed using red blood cell lysis buffer (RBC lysis buffer) before being magnetically sorted using the Anti-Ly6G MicroBeads UltraPure kit (Catalog # 130-120-337, Miltenyi Biotec). T cells were distributed into CD3/CD28 (5ug/ml/1ug/ml) mAb-coated round bottom 96 well plates at 3000 cells per well. Neutrophils were seeded with T cells at a concentration of 4:1. 72 h after co-culture, T cell activation was measured by flow cytometry.

Splenectomy surgery—The surgery was performed three days before DSS treatment. The mice were under anesthesia and the abdominal cavity was opened. The spleen was carefully removed before splenic vessels were cauterized. For sham surgery, the abdomen was opened but the spleen was not removed.

Preparation of Single Cell suspension from tissues

Preparation of mouse colonic cells: Mouse colons were surgically excised, flushed with PBS, then opened longitudinally, and cut into approximately 0.5 cm-long pieces. The colon tissue was washed again with 10 mL PBS followed by incubation in 20 mL HBSS buffer containing 2% FBS, 1mM EDTA, and 1mM DTT in 50 mL canonical tube, at 37°C with

constant shaking at 180 rpm for 20 min to release epithelial cells. The colon tissues were then washed with 10 mL HBSS buffer before being digested in 10 mL 1640 buffer containing 2% FBS, collagenase type II (2 mg/ml), collagenase D (0.5 mg/ml), DispaseII (3 mg/ml) and DNase I (0.1 mg/ml) at 37°C with constant shaking at 180 rpm for 30 min in a 15mL tube. After digestion, the digested cells and remaining tissue fragments were vortexed intensely for 20 s before being passed through a 40 μm cell strainer. The filtered cell suspension was centrifuged at 600g, 4°C for 5 min, then resuspended in 1 mL Facs buffer (2% FBS, 2mM EDTA in DPBS).

Preparation of mouse splenocytes, bone marrow cells, and blood cells: Splenocytes were collected by mashing the spleen by using the plunger end of the syringe in 1 mL Facs buffer. Bone marrow cells were flushed from the femur and tibia bones. Peripheral blood (600–800μL) was collected by retro-orbital bleeding into tubes (BD 365965). Cells were then filtered through a 40μm cell strainer. Cells were centrifuged for 5 min at 500g. The red blood cells were then lysed with RBC lysis buffer for 3 min at room temperature. After centrifugation, cells were washed twice with Facs buffer and resuspended in Facs buffer. For the digestion of spleen CD45$^-$ cells, the spleen capsule was cut into ~1 mm3 fragments using scissors and then digested in spleen digestion solution (200 U/ml DNase I, 250 μg/mL LiberaseDL, 1 mg/mL collagenase, type 4 (Roche) and 500 μg/mL collagenase D (Roche) in HBSS plus Ca^{2+} and Mg^{2+}). After a brief vortex, the spleen fragments were allowed to sediment for ~3 min and the supernatant was transferred to another tube on ice. The sedimented (undigested) spleen fragments were subjected to a second round of digestion. The two fractions of digested cells were pooled and filtered through a 100μm nylon mesh.

Flow cytometry—Single-cell suspensions were analyzed or sorted according to standard protocols using a BD FACS LSRII and BD FACS Aria III (BD Bio-sciences). Flow cytometry was performed as previously described.[68] Cells in single-cell suspension were stained with live-Dead dye (ThermoFisher L34957) for 20 min on ice in the dark. Cells were then fixed with 2% PFA (Santa Cruz, sc-281692). After being washed with a flow cytometry staining buffer (eBioscience, 00-4222-26), cells were first stained with Fc block (BD) for 10 min (except for GMP staining) followed by antibodies for cell-surface markers for 1 h on ice in the dark. The cells were then washed, pelleted, and resuspended in the flow cytometry staining buffer for flow cytometry analysis. The absolute number of cells was counted by using CountBright Absolute Counting Beads (Invitrogen C36950), according to the manufacturer's instruction. Data were analyzed by flowjo.

Single-cell RNA-Sequencing and analysis—Viable cells were used for sequencing following the 10× Genomics protocol. Libraries were prepared using the Single Cell 5′ Library Kit V2 (10× Genomics). Transcriptome profiles of individual cells were determined by 103 Genomics-based droplet sequencing and libraries were sequenced with paired-end reads on an Illumina NovaSeq 6000 (Illumina).

The sequencing reads of the single-cell RNA-seq (scRNA-seq) was mapped to mouse reference (mm10) followed by quantification of transcript expression using cellranger V7.0.0. The single-cell RNA-seq data analysis was performed using Seurat v4.0.1 R package, including cell type stratification and comparative analyses between different

experimental conditions (DKO, WT).[69] In the quality control (QC) analysis, poor-quality cells with <250 (likely cell fragments) or >5,000 (potentially doublets) unique expressed genes were excluded. Cells were removed if their mitochondrial gene percentages were over 10% which indicates poor cell viability. The doublets from the scRNA-seq data were evaluated by DoubletFinder and were removed in the downstream analyses.[70] The data was first merged, normalized, and scaled with default settings in Seurat, followed by principal component analysis (PCA) for dimensionality reduction. We retained 30 leading principal components for further visualization and cell clustering. The Uniform Manifold Approximation and Projection (UMAP) algorithm was used to visualize cells on a two-dimensional space. Subsequently, the share nearest neighbor (SNN) graph was constructed by calculating the Jaccard index between each cell and its 20-nearest neighbors, which was then used for cell clustering based on Louvain algorithm (with a resolution of 0.3). Each cluster was screened for marker genes by differential expression analysis based on the non-parametric Wilcoxon rank-sum test. Based on checking the expression profile of those cluster-specific markers, we identified 8 distinct cell types (including T cells, neutrophils, Mono/Macro, myeloid progenitor cells, two types of B cells, and two types of DCs). In the downstream analysis, we focused on the neutrophil populations which consists of four subclusters. Similarly, we examined the marker profiles of each subcluster to distinguish the functional roles of different neutrophil subtypes. We then specifically identified differentially expressed genes (DEGs) among each sample. Top representative DEGs were visualized using heatmaps or volcano plots. For the analysis of splenic CD45+ cells, 21745 cells were included in our analysis with an average of 1561 genes per cell profiled, resulting in a total of 21373 mouse genes detected in all cells After quality-control processing.

Public data collection and integration—Two independent tumor spleen neutrophil scRNA-seq datasets: GSE139125, GSE163834, and tumor infiltration neutrophil scRNA-seq dataset: GSE213861 were downloaded from Gene Expression Omnibus (GEO) database. Raw sequencing reads were processed and analyzed using cellranger as mentioned above. Seurat was utilized for the down-stream analysis. Batch effect caused by the datasets were assessed and removed using harmony package in R[71]. DEGs among the clusters were identified using FindAllMarker function in Seurat package, where the dataset or batch was regarded as a covariate and was then adjusted. Over-representative pathways of the DEG in the clusters were evaluated by ShinyGO (http://bioinformatics.sdstate.edu/go/). Pathway or gene set scores were calculated by AddModuleScore function in Seurat package.

Mass spectrometry sample preparation and data procession—The cell lysis buffer 10 M urea containing the cOmplete protease inhibitor cocktail (Roche, #11697498001) was used for protein extraction. A VialTweeter device (Hielscher-Ultrasound Technology)[72,73] was used for sonication at 4 °C for two cycle (1 min per cycle), and then centrifuged at 20,000 × g for 1 h to remove the insoluble materials. To break the disulfide bridge and "cap" the cystine, the reduction and alkylation were conducted with 10 mM Dithiothreitol (DTT) for 1 h at 56°C and then 20 mM iodoacetamide (IAA) in dark for 45 min at room temperature. The samples were diluted by 100 mM NH4HCO3 and digested with trypsin (Promega) at ratio of 1:20 (w/w) overnight at 37°C. The digested peptides

purification was performed on C18 column (MarocoSpin Columns, NEST Group INC) and 1 μg of the peptide was injected for mass spectrometry analysis.

The samples were measured by data-independent acquisition (DIA) mass spectrometry method as described previously.[74–76] The Orbitrap Fusion Tribrid Lumos mass spectrometer (Thermo Scientific) instrument coupled to a EASY-nLC 1200 systems (Thermo Scientific, San Jose, CA) was used. The data acquisition was performed with 150-min gradient and 300 nL/min flow rate with the temperature controlled at 60°C using a column oven (PRSO-V1, Sonation GmbH, Biberach, Germany). All the DIA-MS methods consisted of one MS1 scan and 33 MS2 scans of variable isolated windows with 1 m/z overlapping between windows. The MS1 resolution is 120,000 at m/z 200. The MS1 full scan AGC target value was set to be 2E6 and the maximum injection time was 50 ms. The MS2 resolution was set to 30,000 at m/z 200 and the normalized HCD collision energy was 28%. The MS2 AGC was set to be 1.5E6 and the maximum injection time was 50 ms. The default peptide charge state was set to 2. Both MS1 and MS2 spectra were recorded in profile mode. DIA-MS data analysis was performed using Spectronaut v16[77–79] with directDIA algorithm by searching against the SwissProt downloaded mouse fasta file. The oxidation at methionine was set as variable modification, whereas carbamidomethylation at cysteine was set as fixed modification. Both peptide and protein FDR cutoffs (Qvalue) were controlled below 1% and the resulting quantitative data matrix were exported from Spectronaut. All the other settings in Spectronaut were kept as Default.

Knockdown of CD101 in neutrophils—Splenic neutrophils were sorted by the Anti-Ly-6G MicroBeads UltraPure kit (Catalog# 130-120-337, Miltenyi Biotec). Transient transfection of neutrophils was done as previously described.[80] In brief, three million neutrophils were electroporated with 300 nM of SMARTpool ON-TARGETplus siRNA which combines four gene-specific siRNAs into a single reagent pool using the P3 Primary Cell 4D-Nucleofector X Kit (Lonza, Switzerland) under human monocyte nucleofection program with an Amaxa electroporation system. The cells were then cultured for 48 h in the medium supplied with the kit containing 10% FBS and 30 ng/mL recombinant G-CSF (PeproTech, Rocky Hill, NJ).

CD101 recombinant protein suppression assay—Splenic CD8^{+} T cells were sorted using the CD8^{+} T cell isolation kit (Catalog # 130-096-543, Miltenyi Biotec). T cells were allocated to round bottom 96-well plates coated with CD3/CD28 (5ug/ml/1ug/ml) monoclonal antibodies, with recombinant CD101 protein (8.4ug/ml, R&D 3368-CD) or corresponding control protein (8.4ug/ml, R&D 4460-MG-100), at a density of 3000 cells per well. 72 h after co-culture, T cell activation was measured by flow cytometry.

Quantitative RT-PCR—Total RNAs were isolated from cells with the RNeasy Plus mini kit (Qiagen). Complementary DNAs were synthesized from the RNAs with the iScript cDNA synthesis kit (Bio-Rad). Quantitative PCR was done with iTaq Universal SYBR Green Supermix (Bio-Rad). The primer sequences are mouse *Wnt5a* forward: 5′-GGAACGAATCCACGCTAAGGGT-3'; mouse *Wnt5a* reverse: 5′-AGCACGTCTTGAGGCTAC AGGA-3'. mouse *Wnt5b* forward: 5′-GCTACCGCTTTGCCAAGGAGTT-3′ mouse

Wnt5b reverse: 5′-CATTTGCAGGCGACATCAGCCA-3′ mouse *Actin*
forward: 5′-CATTGCTGACAGGATGCAGAAGG-3′ mouse *Actin* reverse:
5′-TGCTGGAAGGTGGACAGTGAGG-3′ mouse *Cxcl12* forward: 5′-
GGAGGATAGATGTGCTCTGGAAC-3′ mouse *Cxcl12* reverse: 5′-
AGTGAGGATGGAGACCGTGGTG-3'

Cell tracing assay—For intra-bone marrow injection, the mice were anesthetized and the hair in the region between the inguen and knee joint was removed using a razor, and a 5-mm incision was made on the thigh. The knee was then flexed to 90°, and the proximal side of the tibia was pulled anteriorly. Next, a 26-gauge needle was inserted through the patellar tendon and into the joint surface of the tibia. The needle was then carefully guided into the bone marrow cavity. To mark the cells, a microsyringe (Hamilton company) containing 40uM of the CFSE dye (Invitrogen) was used to inject 100 μL of dye into the bone marrow cavity via the bone hole. For intra-spleen injection, a left subcostal incision was made to access the peritoneal cavity and expose the spleen. Using a microsyringe (Hamilton company), 50μL of DDAO-SE Far-red dye (40uM) was injected into the spleen. Five different injection sites were carefully chosen to ensure adequate distribution of the dye throughout the spleen. The abdominal muscle and skin were then closed separately using sutures and wound clips, respectively. 2 h after dye injection, mice were sacrificed and bone marrow, blood and spleen cells were collected for flow cytometry analysis. Colon tissue was collected 8 h after dye injection. Before collecting the colon, PE-CD45 antibody was injected through iv 3 min before transcardial perfusion. For flow cytometry analysis of colon infiltrated dye-labeling neutrophils, PE-CD45 positive cells were excluded to eliminate the contamination of circulating cells.[81]

ROS and NET detection in colon neutrophils—ROS and NET were measured by flow cytometry. Colonic single-cell suspensions were obtained from WT mice and DKO mice after DSS treatment. To detect ROS, cells were stained with H2DCFDA ROS dye (Invitrogen) in PBS at 37°C for 15 min, along with a neutrophil marker. For NET detection, cells were first labeled with neutrophil marker dye, then permeabilized using methanol, followed by staining with Cit-Histone3 (abcam ab5103) antibody for 2 h at 4°C, and subsequently stained with a secondary antibody at room temperature for 1 h.

QUANTIFICATION AND STATISTICAL ANALYSIS

Comparisons of means between two groups and multiple groups were tested by unpaired, two-tailed t test and Two-way ANOVA-test using Prism 9.2.0 software (GraphPad). Statistical tests used biological replicates. *p < 0.05, **p < 0.01 and ***p < 0.001 were all considered statistically significant.

Supplementary Material

Refer to Web version on PubMed Central for supplementary material.

ACKNOWLEDGMENTS

REFERENCES

1. Ng LG, Ostuni R, and Hidalgo A (2019). Heterogeneity of neutrophils.Nat. Rev. Immunol. 19, 255–265. 10.1038/s41577-019-0141-8. [PubMed: 30816340]

2. Nicolás-Ávila JÁ, Adrover JM, and Hidalgo A (2017). Neutrophils in Homeostasis, Immunity, and Cancer. Immunity 46, 15–28. 10.1016/j.immuni.2016.12.012.

3. Kolaczkowska E, and Kubes P (2013). Neutrophil recruitment and function in health and inflammation. Nat. Rev. Immunol. 13, 159–175. 10.1038/nri3399. [PubMed: 23435331]

4. Mantovani A, Cassatella MA, Costantini C, and Jaillon S (2011). Neutrophils in the activation and regulation of innate and adaptive immunity. Nat. Rev. Immunol. 11, 519–531. 10.1038/nri3024. [PubMed: 21785456]

5. Nathan C (2006). Neutrophils and immunity: challenges and opportunities. Nat. Rev. Immunol. 6, 173–182. 10.1038/nri1785. [PubMed: 16498448]

6. Burn GL, Foti A, Marsman G, Patel DF, and Zychlinsky A (2021). The Neutrophil. Immunity 54, 1377–1391. 10.1016/j.immuni.2021.06.006. [PubMed: 34260886]

7. Soehnlein O, Steffens S, Hidalgo A, and Weber C (2017). Neutrophilsas protagonists and targets in chronic inflammation. Nat. Rev. Immunol. 17, 248–261. 10.1038/nri.2017.10. [PubMed: 28287106]

8. Ley K, Hoffman HM, Kubes P, Cassatella MA, Zychlinsky A, Hedrick CC, and Catz SD (2018). Neutrophils: New insights and open questions. Sci. Immunol. 3, eaat4579. 10.1126/sciimmunol.aat4579. [PubMed: 30530726]

9. Nauseef WM, and Borregaard N (2014). Neutrophils at work. Nat. Immunol. 15, 602–611. 10.1038/ni.2921. [PubMed: 24940954]

10. Wera O, Lancellotti P, and Oury C (2016). The Dual Role of Neutrophilsin Inflammatory Bowel Diseases. J. Clin. Med. 5. 10.3390/jcm5120118.

11. Fournier BM, and Parkos CA (2012). The role of neutrophils during intestinal inflammation. Mucosal Immunol. 5, 354–366. 10.1038/mi.2012.24. [PubMed: 22491176]

12. Quail DF, Amulic B, Aziz M, Barnes BJ, Eruslanov E, Fridlender ZG, Goodridge HS, Granot Z, Hidalgo A, Huttenlocher A, et al. (2022). Neutrophil phenotypes and functions in cancer: A consensus statement. J. Exp. Med. 219, e20220011. 10.1084/jem.20220011. [PubMed: 35522219]

13. Hedrick CC, and Malanchi I (2022). Neutrophils in cancer: heterogeneous and multifaceted. Nat. Rev. Immunol. 22, 173–187. 10.1038/s41577-021-00571-6. [PubMed: 34230649]

14. Xie X, Shi Q, Wu P, Zhang X, Kambara H, Su J, Yu H, Park SY,Guo R, Ren Q, et al. (2020). Single-cell transcriptome profiling reveals neutrophil heterogeneity in homeostasis and infection. Nat. Immunol. 21, 1119–1133. 10.1038/s41590-020-0736-z. [PubMed: 32719519]

15. Khoyratty TE, Ai Z, Ballesteros I, Eames HL, Mathie S, Martín-Salamanca S, Wang L, Hemmings A, Willemsen N, von Werz V, et al. (2021). Distinct transcription factor networks control neutrophil-driven inflammation. Nat. Immunol. 22, 1093–1106. 10.1038/s41590-021-00968-4. [PubMed: 34282331]

16. Ager A (2023). Cancer immunotherapy: T cells and neutrophils working together to attack cancers. Cell 186, 1304–1306. 10.1016/j.cell.2023.03.005. [PubMed: 37001496]

17. Hirschhorn D, Budhu S, Kraehenbuehl L, Gigoux M, Schröder D, Chow A, Ricca JM, Gasmi B, De Henau O, Mangarin LMB, et al. (2023). T cell immunotherapies engage neutrophils to eliminate tumor antigen escape variants. Cell 186, 1432–1447.e17. 10.1016/j.cell.2023.03.007. [PubMed: 37001503]

18. Gungabeesoon J, Gort-Freitas NA, Kiss M, Bolli E, Messemaker M, Siwicki M, Hicham M, Bill R, Koch P, Cianciaruso C, et al. (2023). A neutrophil response linked to tumor control in immunotherapy. Cell 186, 1448–1464.e20. 10.1016/j.cell.2023.02.032. [PubMed: 37001504]

Author Manuscript   Author Manuscript   Author Manuscript   Author Manuscript

19. Chang JT (2020). Pathophysiology of Inflammatory Bowel Diseases. N. Engl. J. Med. 383, 2652–2664. 10.1056/NEJMra2002697. [PubMed: 33382932]

20. Graham DB, and Xavier RJ (2020). Pathway paradigms revealed from the genetics of inflammatory bowel disease. Nature 578, 527–539. 10.1038/s41586-020-2025-2. [PubMed: 32103191]

21. Adolph TE, Meyer M, Schwärzler J, Mayr L, Grabherr F, and Tilg H (2022). The metabolic nature of inflammatory bowel diseases. Nat. Rev. Gastroenterol. Hepatol. 19, 753–767. 10.1038/s41575-022-00658-y. [PubMed: 35906289]

22. Casalegno Garduño R, and Däbritz J (2021). New Insights on CD8(+) T Cells in Inflammatory Bowel Disease and Therapeutic Approaches. Front. Immunol. 12, 738762. 10.3389/fimmu.2021.738762. [PubMed: 34707610]

23. Corridoni D, Antanaviciute A, Gupta T, Fawkner-Corbett D, Aulicino A, Jagielowicz M, Parikh K, Repapi E, Taylor S, Ishikawa D, et al. (2020). Single-cell atlas of colonic CD8(+) T cells in ulcerative colitis. Nat. Med. 26, 1480–1490. 10.1038/s41591-020-1003-4. [PubMed: 32747828]

24. Nancey S, Holvöet S, Graber I, Joubert G, Philippe D, Martin S, Nicolas JF, Desreumaux P, Flourié B, and Kaiserlian D (2006). CD8+ cytotoxic T cells induce relapsing colitis in normal mice. Gastroenterology 131, 485–496. 10.1053/j.gastro.2006.05.018. [PubMed: 16890603]

25. Lee JC, Lyons PA, McKinney EF, Sowerby JM, Carr EJ, Bredin F, Rickman HM, Ratlamwala H, Hatton A, Rayner TF, et al. (2011). Gene expression profiling of CD8+ T cells predicts prognosis in patients with Crohn disease and ulcerative colitis. J. Clin. Invest. 121, 4170–4179. 10.1172/JCI59255. [PubMed: 21946256]

26. Boschetti G, Nancey S, Moussata D, Cotte E, Francois Y, Flourié B, and Kaiserlian D (2016). Enrichment of Circulating and Mucosal Cytotoxic CD8+ T Cells Is Associated with Postoperative Endoscopic Recurrence in Patients with Crohn's Disease. J. Crohns Colitis 10, 338–345. 10.1093/ecco-jcc/jjv211. [PubMed: 26589954]

27. Jenkins D, Seth R, Kummer JA, Scott BB, Hawkey CJ, and Robins RA (2000). Differential levels of granzyme B, regulatory cytokines, and apoptosis in Crohn's disease and ulcerative colitis at first presentation. J. Pathol. 190, 184–189. 10.1002/(SICI)1096-9896(200002)190:2<184::AID-PATH531>3.0.CO;2-E. [PubMed: 10657017]

28. Kappeler A, and Mueller C (2000). The role of activated cytotoxic T cells in inflammatory bowel disease. Histol. Histopathol. 15, 167–172. 10.14670/HH-15.167. [PubMed: 10668207]

29. Li J, Zaslavsky M, Su Y, Guo J, Sikora MJ, van Unen V, Christophersen A, Chiou SH, Chen L, Li J, et al. (2022). KIR(+)CD8(+) T cells suppress pathogenic T cells and are active in autoimmune diseases and COVID-19. Science 376, eabi9591. 10.1126/science.abi9591. [PubMed: 35258337]

30. Mishra S, Srinivasan S, Ma C, and Zhang N (2021). CD8(+) Regulatory T Cell - A Mystery to Be Revealed. Front. Immunol. 12, 708874. 10.3389/fimmu.2021.708874. [PubMed: 34484208]

31. Koh CH, Lee S, Kwak M, Kim BS, and Chung Y (2023). CD8 T-cell subsets: heterogeneity, functions, and therapeutic potential. Exp. Mol. Med. 55, 2287–2299. 10.1038/s12276-023-01105-x. [PubMed: 37907738]

32. Arosa L, Camba-Gómez M, and Conde-Aranda J (2022). Neutrophils in Intestinal Inflammation: What We Know and What We Could Expect for the Near Future. Gastrointestinal Disorders 4, 263–276. 10.3390/gidisord4040025.

33. Drury B, Hardisty G, Gray RD, and Ho GT (2021). Neutrophil Extra-cellular Traps in Inflammatory Bowel Disease: Pathogenic Mechanisms and Clinical Translation. Cell. Mol. Gastroenterol. Hepatol. 12, 321–333. 10.1016/j.jcmgh.2021.03.002. [PubMed: 33689803]

34. Gavin BJ, McMahon JA, and McMahon AP (1990). Expression of multiple novel Wnt-1/int-1-related genes during fetal and adult mouse development. Genes Dev. 4, 2319–2332. 10.1101/gad.4.12b.2319. [PubMed: 2279700]

35. Mastelaro de Rezende M, Zenker Justo G, Julian Paredes-Gamero E, and Gosens R (2020). Wnt-5A/B Signaling in Hematopoiesis throughout Life. Cells 9, 1801. 10.3390/cells9081801. [PubMed: 32751131]

36. Rogers S, and Scholpp S (2022). Vertebrate Wnt5a - At the crossroads of cellular signalling. Semin. Cell Dev. Biol. 125, 3–10. 10.1016/j.semcdb.2021.10.002. [PubMed: 34686423]

37. Suthon S, Perkins RS, Bryja V, Miranda-Carboni GA, and Krum SA (2021). WNT5B in Physiology and Disease. Front. Cell Dev. Biol. 9, 667581. 10.3389/fcell.2021.667581. [PubMed: 34017835]

38. Agalliu D, Takada S, Agalliu I, McMahon AP, and Jessell TM (2009). Motor neurons with axial muscle projections specified by Wnt4/5 signaling. Neuron 61, 708–720. 10.1016/j.neuron.2008.12.026. [PubMed: 19285468]

39. Minegishi K, Hashimoto M, Ajima R, Takaoka K, Shinohara K, Ikawa Y, Nishimura H, McMahon AP, Willert K, Okada Y, et al. (2017). A Wnt5 Activity Asymmetry and Intercellular Signaling via PCP Proteins Polarize Node Cells for Left-Right Symmetry Breaking. Dev. Cell 40, 439–452.e4. 10.1016/j.devcel.2017.02.010. [PubMed: 28292423]

40. Kessenbrock K, Smith P, Steenbeek SC, Pervolarakis N, Kumar R, Minami Y, Goga A, Hinck L, and Werb Z (2017). Diverse regulation of mammary epithelial growth and branching morphogenesis through non-canonical Wnt signaling. Proc. Natl. Acad. Sci. USA 114, 3121–3126. 10.1073/pnas.1701464114. [PubMed: 28270600]

41. Miyoshi H, Ajima R, Luo CT, Yamaguchi TP, and Stappenbeck TS (2012). Wnt5a potentiates TGF-beta signaling to promote colonic crypt regeneration after tissue injury. Science 338, 108–113. 10.1126/science.1223821. [PubMed: 22956684]

42. Sato A, Kayama H, Shojima K, Matsumoto S, Koyama H, Minami Y, Nojima S, Morii E, Honda H, Takeda K, and Kikuchi A (2015). The Wnt5a-Ror2 axis promotes the signaling circuit between interleukin-12 and interferon-gamma in colitis. Sci. Rep. 5, 10536. 10.1038/srep10536. [PubMed: 26030277]

43. Evrard M, Kwok IWH, Chong SZ, Teng KWW, Becht E, Chen J, Sieow JL, Penny HL, Ching GC, Devi S, et al. (2018). Developmental Analysis of Bone Marrow Neutrophils Reveals Populations Specialized in Expansion, Trafficking, and Effector Functions. Immunity 48, 364–379.e8. 10.1016/j.immuni.2018.02.002. [PubMed: 29466759]

44. Crane GM, Jeffery E, and Morrison SJ (2017). Adult haematopoietic stem cell niches. Nat. Rev. Immunol. 17, 573–590. 10.1038/nri.2017.53. [PubMed: 28604734]

45. Comazzetto S, Shen B, and Morrison SJ (2021). Niches that regulate stem cells and hematopoiesis in adult bone marrow. Dev. Cell 56, 1848–1860. 10.1016/j.devcel.2021.05.018. [PubMed: 34146467]

46. Sugiyama T, Kohara H, Noda M, and Nagasawa T (2006). Maintenance of the hematopoietic stem cell pool by CXCL12-CXCR4 chemokine signaling in bone marrow stromal cell niches. Immunity 25, 977–988. 10.1016/j.immuni.2006.10.016. [PubMed: 17174120]

47. Wrage M, Kaltwasser J, Menge S, and Mattner J (2021). CD101 as an indicator molecule for pathological changes at the interface of host-microbiota interactions. Int. J. Med. Microbiol. 311, 151497. 10.1016/j.ijmm.2021.151497. [PubMed: 33773220]

48. Schey R, Dornhoff H, Baier JLC, Purtak M, Opoka R, Koller AK, Atreya R, Rau TT, Daniel C, Amann K, et al. (2016). CD101 inhibits the expansion of colitogenic T cells. Mucosal Immunol. 9, 1205–1217. 10.1038/mi.2015.139. [PubMed: 26813346]

49. Alshetaiwi H, Pervolarakis N, McIntyre LL, Ma D, Nguyen Q, Rath JA, Nee K, Hernandez G, Evans K, Torosian L, et al. (2020). Defining the emergence of myeloid-derived suppressor cells in breast cancer using single-cell transcriptomics. Sci. Immunol. 5, eaay6017. 10.1126/sciimmunol.aay6017. [PubMed: 32086381]

50. Veglia F, Hashimoto A, Dweep H, Sanseviero E, De Leo A, Tcyganov E, Kossenkov A, Mulligan C, Nam B, Masters G, et al. (2021). Analysis of classical neutrophils and polymorphonuclear myeloid-derived suppressor cells in cancer patients and tumor-bearing mice. J. Exp. Med. 218, e20201803. 10.1084/jem.20201803. [PubMed: 33566112]

51. Kim R, Hashimoto A, Markosyan N, Tyurin VA, Tyurina YY, Kar G, Fu S, Sehgal M, Garcia-Gerique L, Kossenkov A, et al. (2022). Ferroptosis of tumour neutrophils causes immune suppression in cancer. Nature 612, 338–346. 10.1038/s41586-022-05443-0. [PubMed: 36385526]

52. Gullotta GS, De Feo D, Friebel E, Semerano A, Scotti GM, Bergamaschi A, Butti E, Brambilla E, Genchi A, Capotondo A, et al. (2023). Age-induced alterations of granulopoiesis generate atypical neutrophils that aggravate stroke pathology. Nat. Immunol. 24, 925–940. 10.1038/s41590-023-01505-1. [PubMed: 37188941]

53. Caiado F, Pietras EM, and Manz MG (2021). Inflammation as a regulator of hematopoietic stem cell function in disease, aging, and clonal selection. J. Exp. Med. 218, e20201541. 10.1084/jem.20201541. [PubMed: 34129016]

54. Fernández-García V, Gonzá lez-Ramos S., Martín-Sanz P., Castrillo A., and Boscá L. (2020). Contribution of Extramedullary Hematopoiesis to Atherosclerosis. The Spleen as a Neglected Hub of Inflammatory Cells. Front. Immunol. 11, 586527. 10.3389/fimmu.2020.586527. [PubMed: 33193412]

55. Kawashima K, Onizawa M, Fujiwara T, Gunji N, Imamura H, Katakura K, and Ohira H (2022). Evaluation of the relationship between the spleen volume and the disease activity in ulcerative colitis and Crohn disease. Medicine (Baltim.) 101, e28515. 10.1097/MD.0000000000028515.

56. Kim CH (2010). Homeostatic and pathogenic extramedullary hematopoiesis. J. Blood Med. 1, 13–19. 10.2147/JBM.S7224. [PubMed: 22282679]

57. Chassaing B, Aitken JD, Malleshappa M, and Vijay-Kumar M (2014). Dextran sulfate sodium (DSS)-induced colitis in mice. Curr. Protoc. Immunol. 104, 15.25.1–15.25.14. 10.1002/0471142735.im1525s104.

58. Wu C, Ning H, Liu M, Lin J, Luo S, Zhu W, Xu J, Wu WC, Liang J, Shao CK, et al. (2018). Spleen mediates a distinct hematopoietic progenitor response supporting tumor-promoting myelopoiesis. J. Clin. Invest. 128, 3425–3438. 10.1172/JCI97973. [PubMed: 29771686]

59. Cortez-Retamozo V, Etzrodt M, Newton A, Rauch PJ, Chudnovskiy A, Berger C, Ryan RJH, Iwamoto Y, Marinelli B, Gorbatov R, et al. (2012). Origins of tumor-associated macrophages and neutrophils. Proc. Natl. Acad. Sci. USA 109, 2491–2496. 10.1073/pnas.1113744109. [PubMed: 22308361]

60. Veglia F, Sanseviero E, and Gabrilovich DI (2021). Myeloid-derived suppressor cells in the era of increasing myeloid cell diversity. Nat. Rev. Immunol. 21, 485–498. 10.1038/s41577-020-00490-y. [PubMed: 33526920]

61. Veglia F, Perego M, and Gabrilovich D (2018). Myeloid-derived suppressor cells coming of age. Nat. Immunol. 19, 108–119. 10.1038/s41590-017-0022-x. [PubMed: 29348500]

62. Hegde S, Leader AM, and Merad M (2021). MDSC: Markers, development, states, and unaddressed complexity. Immunity 54, 875–884. 10.1016/j.immuni.2021.04.004. [PubMed: 33979585]

63. Gong Z, Li Q, Shi J, Li P, Hua L, Shultz LD, and Ren G (2023). Immunosuppressive reprogramming of neutrophils by lung mesenchymal cells promotes breast cancer metastasis. Sci. Immunol. 8, eadd5204. 10.1126/sciimmunol.add5204. [PubMed: 36800412]

64. Mousset A, Lecorgne E, Bourget I, Lopez P, Jenovai K, Cherfils-Vicini J, Dominici C, Rios G, Girard-Riboulleau C, Liu B, et al. (2023). Neutrophil extracellular traps formed during chemotherapy confer treatment resistance via TGF-beta activation. Cancer Cell 41, 757–775.e10. 10.1016/j.ccell.2023.03.008. [PubMed: 37037615]

65. Linde IL, Prestwood TR, Qiu J, Pilarowski G, Linde MH, Zhang X, Shen L, Reticker-Flynn NE, Chiu DKC, Sheu LY, et al. (2023). Neutrophil-activating therapy for the treatment of cancer. Cancer Cell 41, 356–372.e10. 10.1016/j.ccell.2023.01.002. [PubMed: 36706760]

66. Adrover JM, McDowell SAC, He XY, Quail DF, and Egeblad M (2023). NETworking with cancer: The bidirectional interplay between cancer and neutrophil extracellular traps. Cancer Cell 41, 505–526. 10.1016/j.ccell.2023.02.001. [PubMed: 36827980]

67. Garo LP, Ajay AK, Fujiwara M, Beynon V, Kuhn C, Gabriely G, Sadhukan S, Raheja R, Rubino S, Weiner HL, and Murugaiyan G (2019). Smad7 Controls Immunoregulatory PDL2/1-PD1 Signaling in Intestinal Inflammation and Autoimmunity. Cell Rep. 28, 3353–3366.e5. 10.1016/j.celrep.2019.07.065. [PubMed: 31553906]

68. Luan Y, Yuan Q, Wang Q, Compton S, Wu D, and Tang W (2022). Pazopanib Is a Potential Treatment for Coronavirus-Induced Lung Injuries. J. Immunol. 209, 723–730. 10.4049/jimmunol.2100968. [PubMed: 35914834]

69. Stuart T, Butler A, Hoffman P, Hafemeister C, Papalexi E, Mauck WM 3rd, Hao Y, Stoeckius M, Smibert P, and Satija R (2019). Comprehensive Integration of Single-Cell Data. Cell 177, 1888–1902.e21. 10.1016/j.cell.2019.05.031. [PubMed: 31178118]

70. DePasquale EAK, Schnell DJ, Van Camp PJ, Valiente-Alandí í, Blaxall BC., Grimes HL., Singh H., and Salomonis N. (2019). Double-tDecon: Deconvoluting Doublets from Single-Cell RNA-Sequencing Data. Cell Rep. 29, 1718–1727.e8. 10.1016/j.celrep.2019.09.082. [PubMed: 31693907]

71. Korsunsky I, Millard N, Fan J, Slowikowski K, Zhang F, Wei K, Baglaenko Y, Brenner M, Loh PR, and Raychaudhuri S (2019). Fast, sensitive and accurate integration of single-cell data with Harmony. Nat. Methods 16, 1289–1296. 10.1038/s41592-019-0619-0. [PubMed: 31740819]

72. Liu Y, Beyer A, and Aebersold R (2016). On the Dependency of Cellular Protein Levels on mRNA Abundance. Cell 165, 535–550. 10.1016/j.cell.2016.03.014. [PubMed: 27104977]

73. Collins BC, Hunter CL, Liu Y, Schilling B, Rosenberger G, Bader SL, Chan DW, Gibson BW, Gingras A-C, Held JM, et al. (2017). Multi-laboratory assessment of reproducibility, qualitative and quantitative performance of SWATH-mass spectrometry. Nat. Commun. 8, 291. 10.1038/s41467-017-00249-5. [PubMed: 28827567]

74. Mehnert M, Li W, Wu C, Salovska B, and Liu Y (2019). Combining Rapid Data Independent Acquisition and CRISPR Gene Deletion for Studying Potential Protein Functions: A Case of HMGN1. Proteomics 19, e1800438. 10.1002/pmic.201800438. [PubMed: 30901150]

75. Li W, Chi H, Salovska B, Wu C, Sun L, Rosenberger G, and Liu Y (2019). Assessing the Relationship Between Mass Window Width and Retention Time Scheduling on Protein Coverage for Data-Independent Acquisition. J. Am. Soc. Mass Spectrom. 30, 1396–1405. 10.1007/s13361-019-02243-1. [PubMed: 31147889]

76. Liu Y, Mi Y, Mueller T, Kreibich S, Williams EG, Van Drogen A, Borel C, Frank M, Germain P-L, Bludau I, et al. (2019). Multi-omic measurements of heterogeneity in HeLa cells across laboratories. Nat. Biotechnol. 37, 314–322. 10.1038/s41587-019-0037-y. [PubMed: 30778230]

77. Bruderer R, Bernhardt OM, Gandhi T, Miladinovic SM, Cheng LY, Messner S, Ehrenberger T, Zanotelli V, Butscheid Y, Escher C, et al. (2015). Extending the limits of quantitative proteome profiling with data-independent acquisition and application to acetaminophen-treated three-dimensional liver microtissues. Mol. Cell. Proteomics 14, 1400–1410. 10.1074/mcp.M114.044305. [PubMed: 25724911]

78. Bruderer R, Bernhardt OM, Gandhi T, Xuan Y, Sondermann J, Schmidt M, Gomez-Varela D, and Reiter L (2017). Optimization of Experimental Parameters in Data-Independent Mass Spectrometry Significantly Increases Depth and Reproducibility of Results. Mol. Cell. Proteomics 16, 2296–2309. 10.1074/mcp.RA117.000314. [PubMed: 29070702]

79. Salovska B, Zhu H, Gandhi T, Frank M, Li W, Rosenberger G, Wu C, Germain P-L, Zhou H, Hodny Z, et al. (2020). Isoform-resolved correlation analysis between mRNA abundance regulation and protein level degradation. Mol. Syst. Biol. 16, e9170. 10.15252/msb.20199170. [PubMed: 32175694]

80. Ren C, Yuan Q, Braun M, Zhang X, Petri B, Zhang J, Kim D, Guez-Haddad J, Xue W, Pan W, et al. (2019). Leukocyte Cytoskeleton Polarization Is Initiated by Plasma Membrane Curvature from Cell Attachment. Dev. Cell 49, 206–219.e7. 10.1016/j.devcel.2019.02.023. [PubMed: 30930167]

81. Reilly EC, Lambert Emo K, Buckley PM, Reilly NS, Smith I, Chaves FA, Yang H, Oakes PW, and Topham DJ (2020). T(RM) integrins CD103 and CD49a differentially support adherence and motility after resolution of influenza virus infection. Proc. Natl. Acad. Sci. USA 117, 12306–12314. 10.1073/pnas.1915681117. [PubMed: 32439709]

Highlights

- Loss of WNT5 protects mice from colitis by promoting splenic granulopoiesis

- WNT5 proteins constitute negative feedback control of splenic granulopoiesis during colitis

- Splenic granulopoiesis produces hyper-immunosuppressive and hypo-pro-inflammatory neutrophils
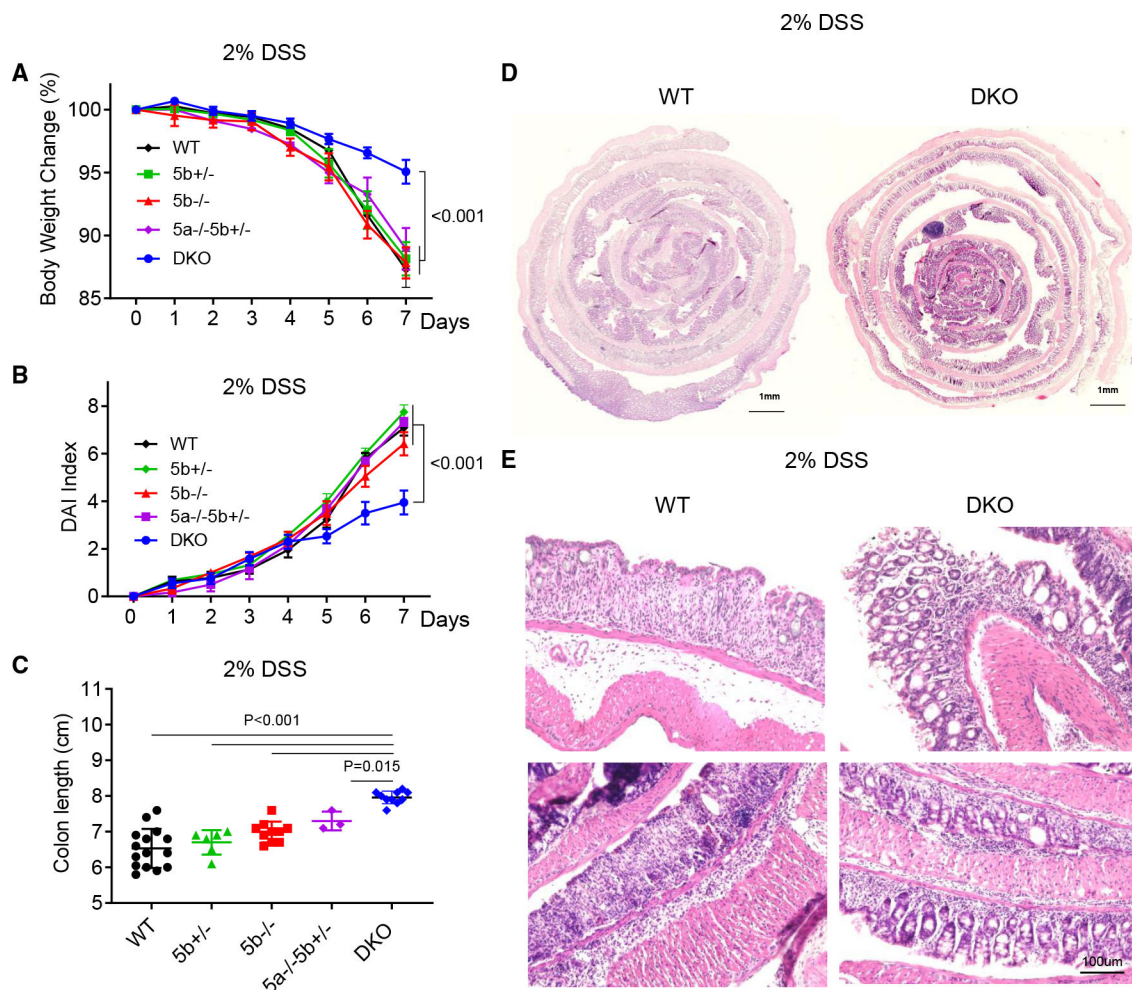
Figure 1. Loss of WNT5 protects mice from DSS-induced colitis

Wnt5a and *Wnt5b* double knockout (DKO) mice (n = 9) and various control mice (WT, n = 13; *Wnt5b*$^{+/-}$, n = 7; *Wnt5b*$^{-/-}$, n = 8; *Wnt5b*$^{-/-}$*Wnt5b*$^{+/-}$, n = 3) were treated with DSS in drinking water for 7 days. Body weight was monitored daily, and the percentage of body weight loss is shown in (A). Disease activity index was assessed daily and is shown in (B). Colons were collected and analyzed on day 7 of DSS treatment, and colon length is shown in (C). Representative sections of the Swiss rolls from the colons of WT mice and DKO mice stained with hematoxylin and eosin (H&E) are shown in (D), and higher-magnification views of the colon are shown in (E). In (C), each datum represents one mouse. Results in (A)–(C) are presented as means ± SEM with p values (two-tailed one-way ANOVA). Each independent experiment consists of at least three technical replicates. See also Figure S1.
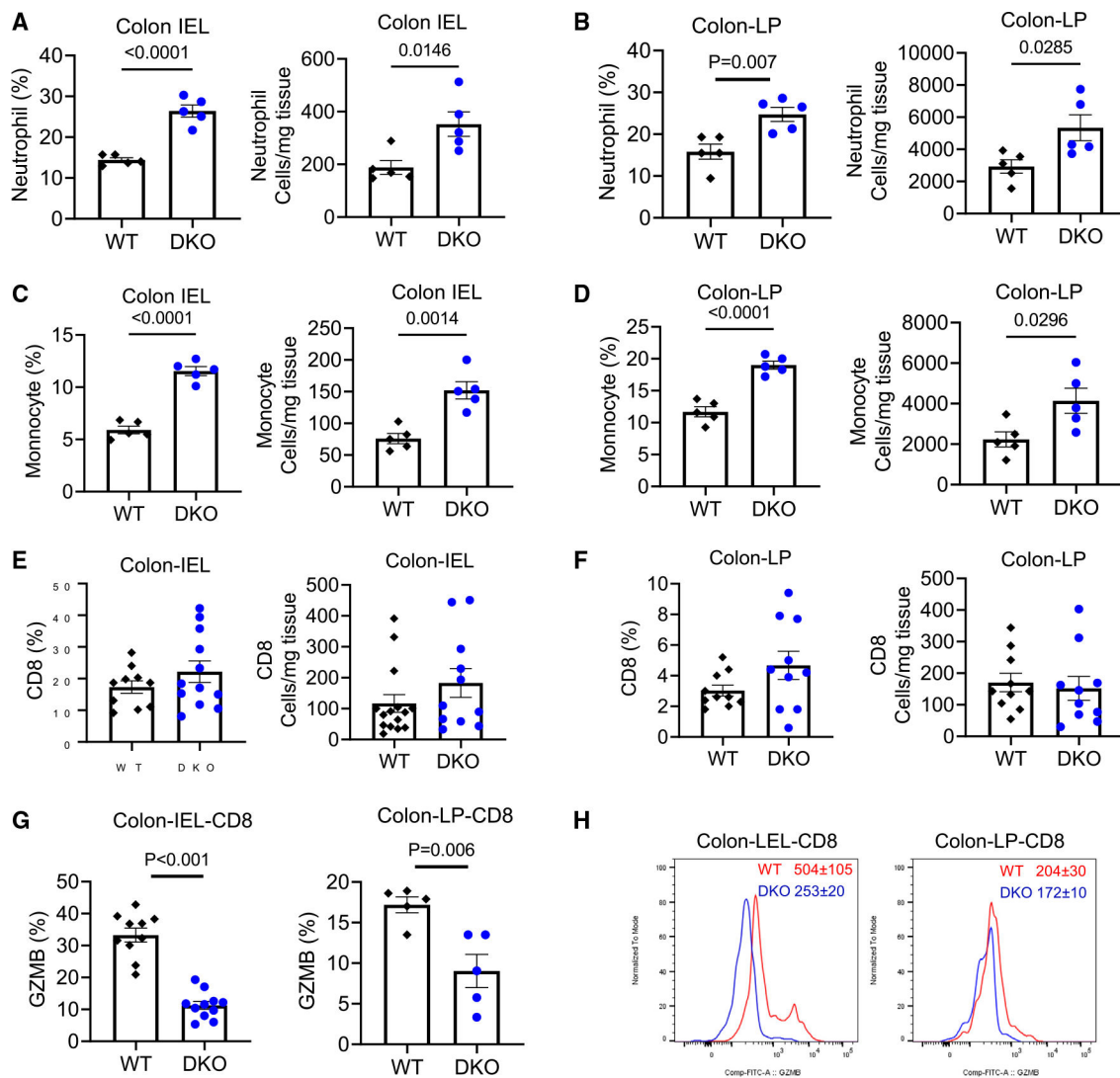
Figure 2. Loss of WNT5 results in myeloid cell expansion and suppression of GZMB$^+$ CD8$^+$ T cells in colitic colons

The *Wnt5* DKO mice and WT control mice were treated as in Figure 1. Cells were isolated from the colon intraepithelial layer (IEL) and laminae propria (LP).

(A–F) The percentages of leukocyte populations in the CD45$^+$ population and their absolute numbers were determined by flow cytometry.

(G and H) The percentages of GZMB$^+$ in CD8$^+$ T cells and mean fluorescence intensity of GZMB in CD8$^+$ T cells together with representative flow cytometry charts are shown.

Data in (A)–(G) are presented as means ± SEM with p values (two-tailed Student's t test). Each datum point represents one mouse. Each independent experiment consists of at least three technical replicates.
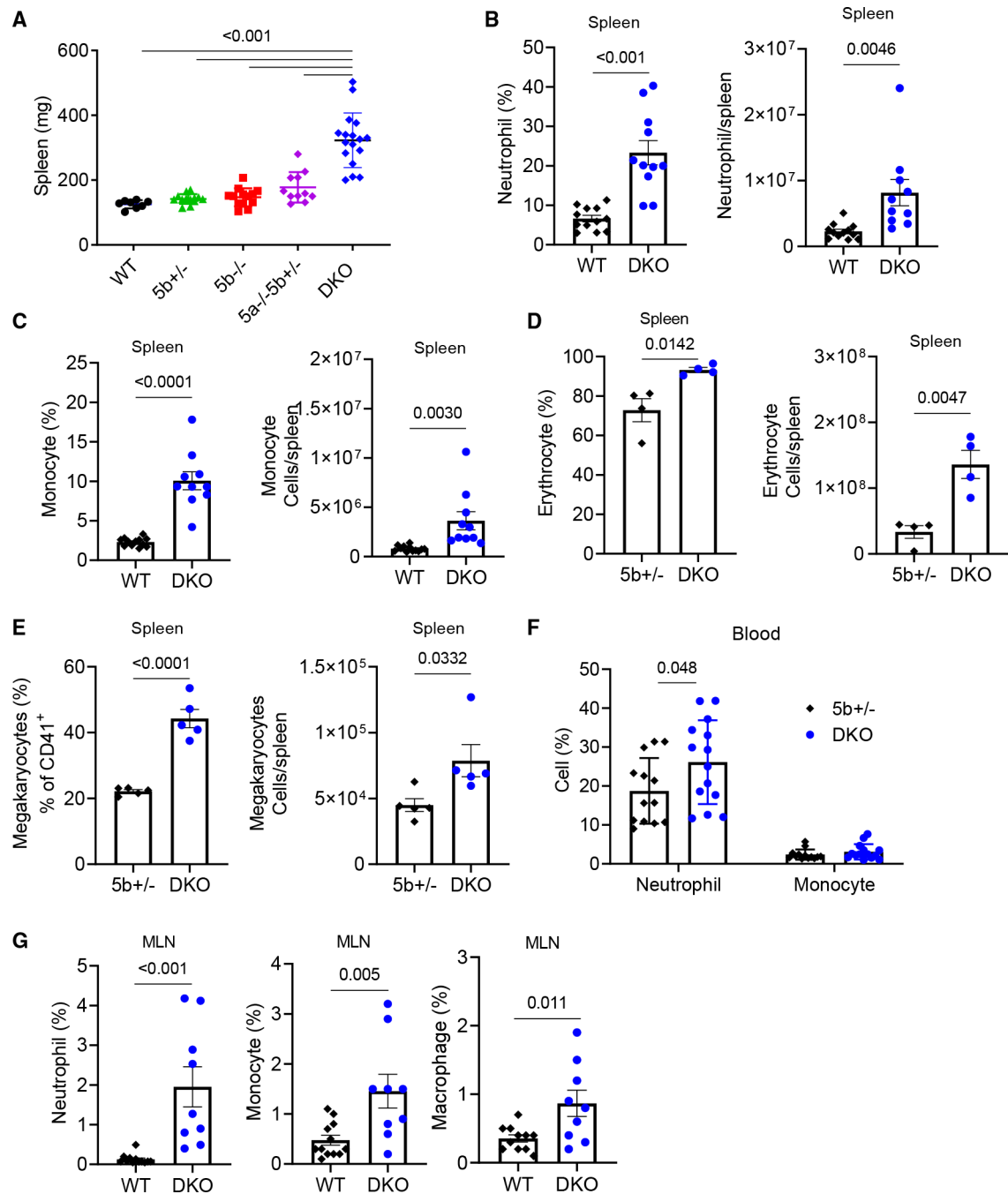
See also Figure S2.

Figure 3. Colitic *Wnt5* DKO mice develop splenomegaly

Mice were treated as in Figure 1, and samples were collected on day 7 of DSS treatment.

(A) Spleen weight is shown.

(B and C) The percentages of neutrophils and monocytes in the CD45+ population and their absolute numbers were determined by flow cytometry.

(D) The percentages of erythrocytes in the CD45− population and their absolute numbers were determined by flow cytometry.

(E) The percentages of megakaryocytes in the $CD45^-CD150^+CD41^+$ population and their absolute numbers were determined by flow cytometry.

(F and G) The percentages of neutrophils, monocytes, and macrophages in the $CD45^+$ population were determined by flow cytometry.

Data are presented as means ± SEM with p value (two-tailed one-way ANOVA for A; two-tailed Student's t test for B–G). Each datum point represents one mouse. Each independent experiment consists of at least three technical replicates.
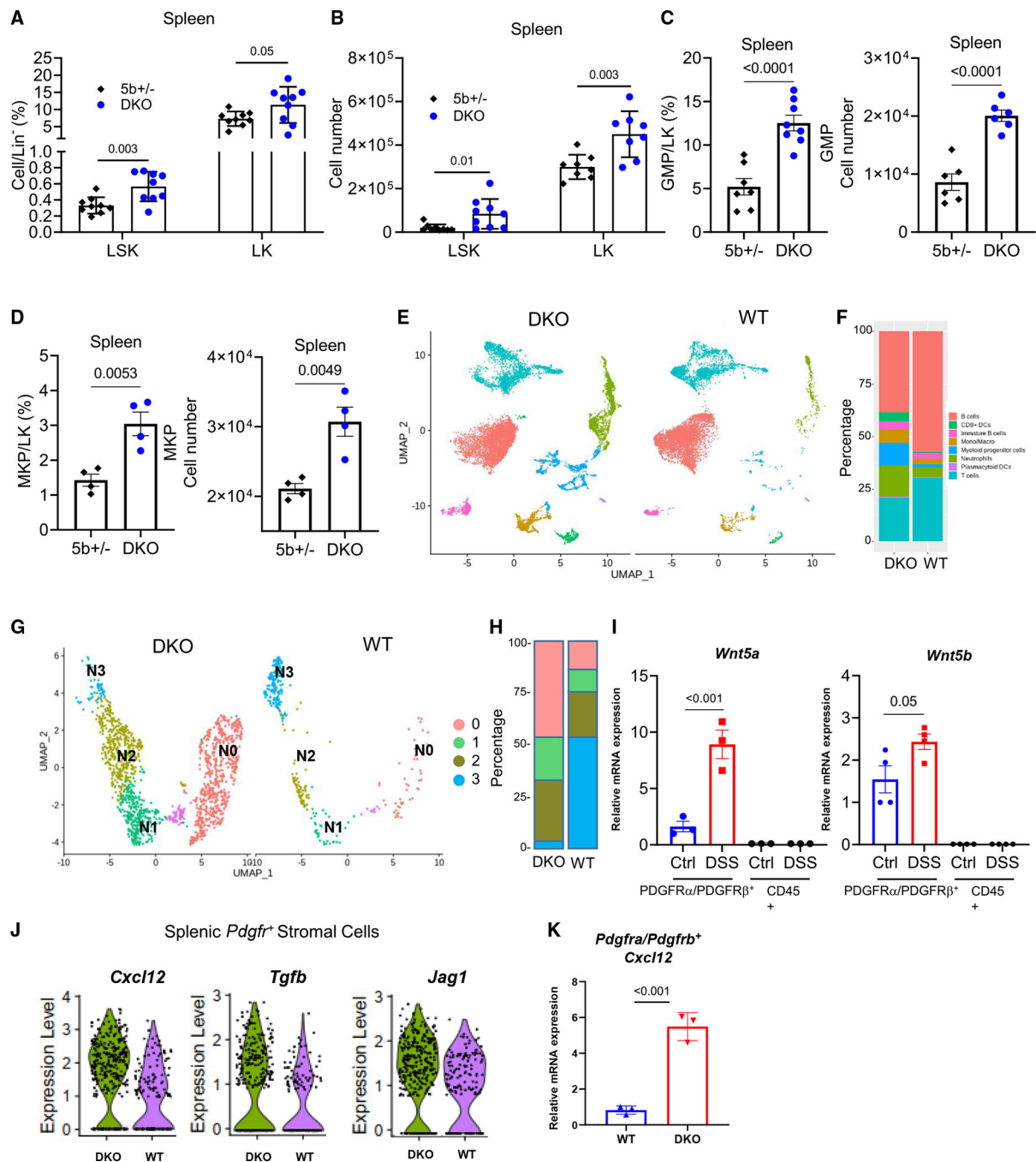
See also Figure S3.

Figure 4. *Wnt5* DKO mice enhance splenic extramedullary hematopoiesis upon colitis induction

(A–F) DKO mice and WT control mice were treated as Figure 1. The percentages of LK and LSK cells in Lineage$^-$ and their absolute numbers were determined by flow cytometry (A and B). The percentages of GMPs and MKPs in LK and their absolute numbers were determined by flow cytometry (C and D).

(E) Uniform maniform approximation and projection (UMAP) plots of splenic CD45$^+$ cells from DSS-treated *Wnt5* DKO mice and WT mice.

(F) Percentages of the major cell types identified in (E).

(G) UMAP plots of the subclusters of cells expressing $Ly6g^+$, $S100a8^+$, and/or $Cxcr2^+$ neutrophil markers from DSS-treated *Wnt5* DKO mice and WT mice.

(H) Percentages of the subclusters identified in (G).

(I) WT mice were treated with normal water or DSS water for 7 days, and *Wnt5a* and *Wnt5b* mRNA expressions were determined by RT-qPCR in splenic $CD45^+$ cells and $CD45PDGFR\alpha^+PDGFR\beta^+$ cells.

(J) WT mice and *Wnt5* DKO mice were treated as in Figure 1. Spleen $CD45^-$ cells were collected and subjected to single-cell RNA sequencing (scRNA-seq). Expressions of *Cxcl12*, *Jag1*, and *Tgfb* in the $PDGFR\alpha/PDGFR\beta^+$ cells of WT mice and DKO mice are shown in (J).

(K) WT and *Wnt5* DKO mice were treated as in Figure 1. Spleen $CD45^-PDGFR\alpha^+PDGFR\beta^+$ cells were collected, and *Cxcl12* mRNA expression was detected. Results in (A)–(D), (I), and (K) are shown as means ± SEM with p values (two-tailed Student's t test). Each datum point represents one mouse. Each independent experiment consists of at least three technical replicates.

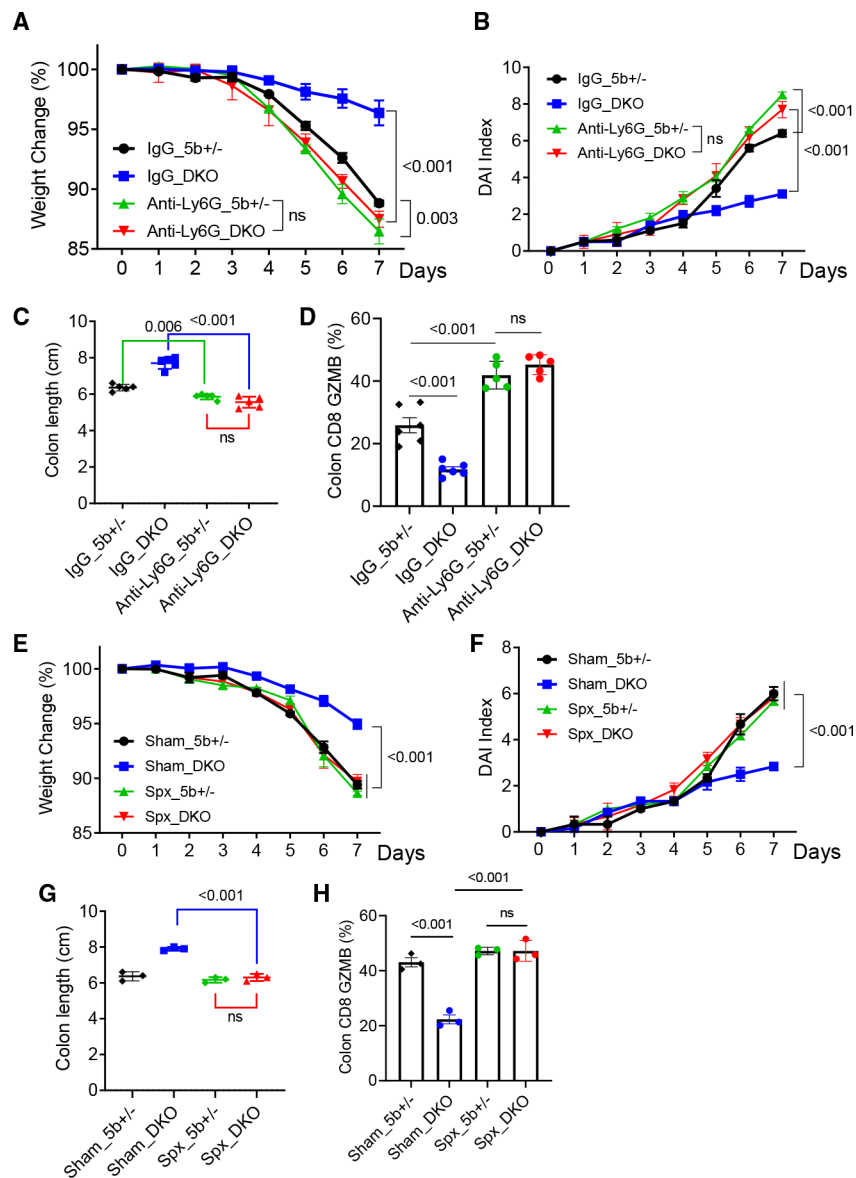See also Figure S4 and Tables S1 and S2.

Figure 5. Colitic phenotypes of *Wnt5* DKO mice depend on splenic neutrophils

(A–D) *Wnt5* DKO mice and the control mice were treated with DSS and subjected to neutrophil depletion as shown in Figure S5A (n = 5). Colitic phenotypes are shown in (A)–(C), and the percentages of GZMB$^+$ in colon CD8$^+$ T cells were determined by flow cytometry (D).

(E–H) *Wnt5* DKO mice and the control mice were subjected to splenectomy before being treated with DSS (n = 3). Colitic phenotypes are shown in (E)–(G). Percentages of GZMB$^+$ in colon CD8$^+$ T cells were determined by flow cytometry (H).

Data are presented as means ± SEM with p values (two-tailed two-way ANOVA). Each datum point in (C), (D), (G), and (H) represents one mouse. Each independent experiment consists of at least three technical replicates.
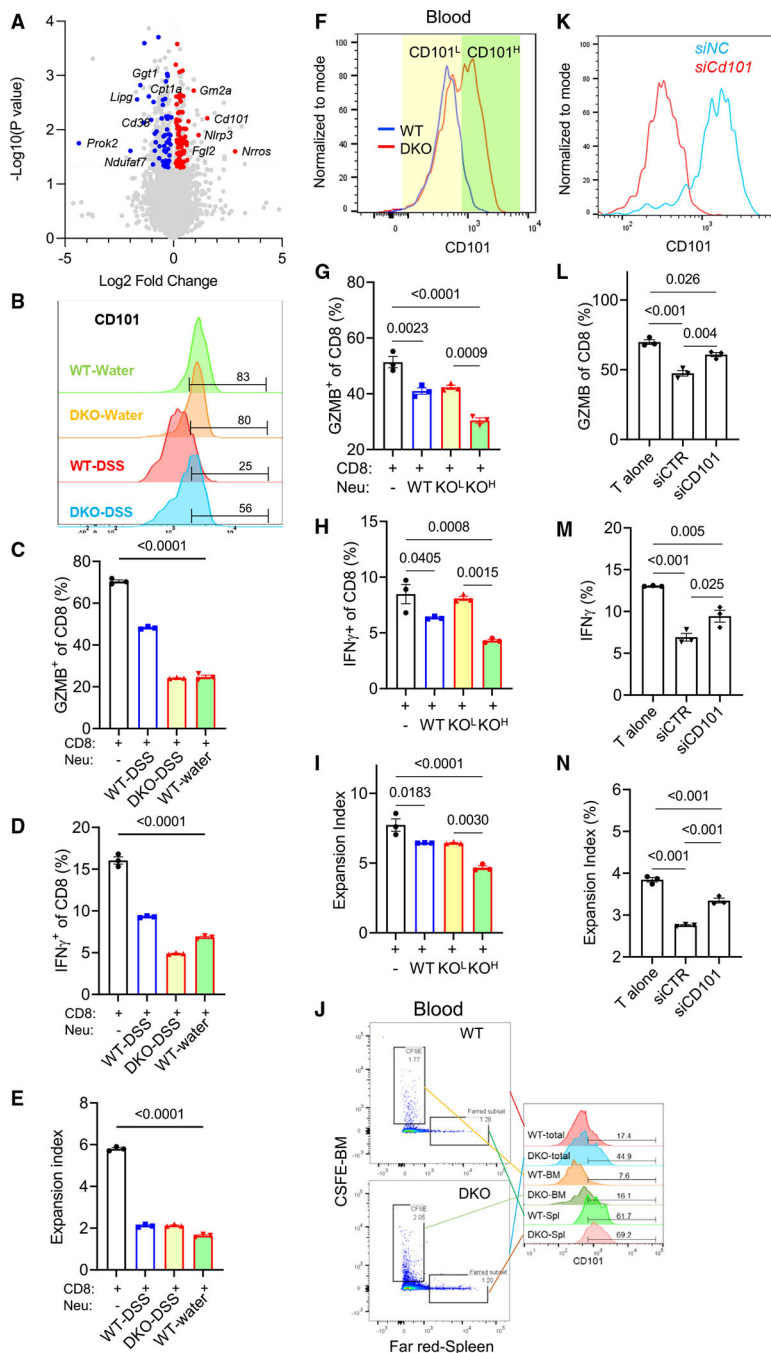
See also Figure S5.

Figure 6. Colitic *Wnt5* DKO mice produce CD101-high hyper-immunosuppressive neutrophils from the spleen

DKO mice and WT control mice were treated as in Figure 1.

(A) Common upregulated (red) and downregulated (blue) genes (log2 fold change > 0.1 or < −0.1, adjusted p value [p value adj] < 0.05) from transcriptomic and proteomic analyses of blood neutrophils from DKO mice and WT mice are denoted on the volcano plot.

(B) CD101 was detected by flow cytometry in blood neutrophils from DKO mice and WT control mice treated with water or DSS.

(C–E) CD8$^+$ T cells were cocultured with blood neutrophils sorted from WT water, WT-DSS, and DKO-DSS mice for 72 h. GZMB, interferon γ (IFNγ), and T cell expansion were determined by flow cytometry.

(F–I) CD8$^+$ T cells were cocultured with WT-DSS blood neutrophils and DKO-DSS CD101-low and DKO-DSS CD101-high blood neutrophils, respectively, for 72 h. GZMB, IFNγ, and T cell expansion were determined by flow cytometry. Colored shades denote fluorescence-activated cell sorting (FACS) gating.

(J) CD101 expression was determined in blood Ly6G$^+$CFSE$^+$ and Ly6G$^+$Far-Red$^+$ cells by flow cytometry.

(K–N) Splenic neutrophils from WT-DSS mice and DKO-DSS mice were isolated by FACS and transfected with the *Cd101* small interfering RNA (siRNA) for 48 h and then cocultured with CD8$^+$ T cells for 72 h. The knockdown efficiency of *Cd101* is shown in (K). GZMB, IFNγ, and T cell expansion were determined by flow cytometry.

Data in (C)–(E), (G)–(I) and (L)–(N) are presented as means ± SEM with p values (two-tailed one-way ANOVA), and each datum point represents one mouse. Each independent experiment consists of at least three technical replicates.

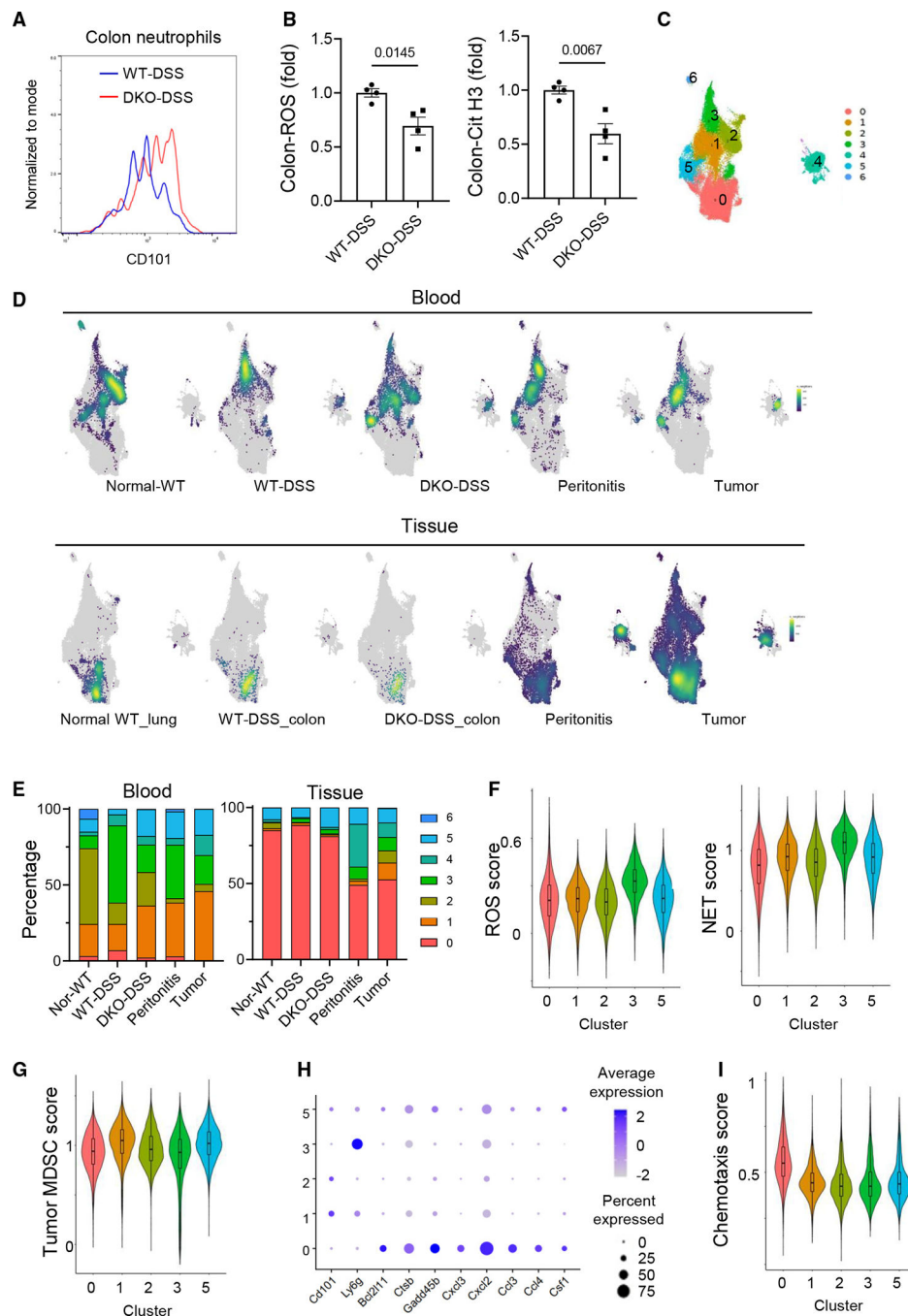See also Figure S6, Tables S3, S4, S5, and S6.

Figure 7. Transcriptomic profiles of blood neutrophils inform the functions of colon neutrophils

(A) CD101 expression in the colon neutrophils of the WT-DSS mice and DKO-DSS mice was determined by flow cytometry.

(B) The ROS and citrullinated histone 3 (Cit-H3) contents in the colon neutrophils were determined by flow cytometry, and data are presented as means ± SEM with p values (two-tailed Student's t test). Each datum point represents one mouse. Each independent experiment consists of at least three technical replicates.

(C) UMAP projection of subclusters of neutrophils aggregated from different scRNA-seq datasets.

(D) Point density-plot visualization of neutrophil distributions under different conditions. The color represents the density of overlapped neutrophils in local regions.

(E) Percentages of the subclusters under different conditions.

(F, G, and I) Violin plots of the ROS score, NET score, MDSC score, and chemotaxis score for the major subclusters.

(H) Expression of selected genes in the major subclusters.

See also Figure S7, Tables S7, S8, and S9.

KEY RESOURCES TABLE

REAGENT or RESOURCE	SOURCE	IDENTIFIER
Antibodies		
Anti-mouse Ly6C	BioLegend	Cat#128008; RRID:AB_1186132
Anti-mouse Ly6G	BioLegend	Cat#127612; RRID:AB_2251161
Anti-mouse B220	BioLegend	Cat#103208; RRID:AB_312993
Anti-mouse MHCII	Thermo Scientific	Cat#48-5321-80; RRID:AB_1272241
Anti-mouse CD11c	BioLegend	Cat#117307; RRID:AB_313776
Anti-mouse CD64	BioLegend	Cat#139315; RRID:AB_2566555
Anti-mouse CD11b	BioLegend	Cat#101207; RRID:AB_312791
Anti-mouse CD45	BD Biosciences	Cat#564279; RRID:AB_2651134
Anti-mouse TCR alpha/beta	Biolegend	Cat#109211; RRID:AB_313434
Anti-mouse CD8a	BD Biosciences	Cat#563786; RRID:AB_2732919
Anti-mouse CD4	BioLegend	Cat#100534; RRID:AB_493374
Anti-mouse TCR gamma/delta	ThermoFisher	Cat#12-5711-81; RRID:AB_465933
Anti-mouse Granzyme B	Biolegend	Cat#515403; RRID:AB_2114575
Anti-mouse IFNgamma	ThermoFisher	Cat#12-7311-82; RRID:AB_466193
Anti-mouse Foxp3	ThermoFisher	Cat#11-5773-82; RRID:AB_465243
Anti-mouse IL17	BioLegend	Cat#506916; RRID:AB_536017
Anti-mouse Lineage cocktail	BioLegend	Cat#133310; RRID:AB_11150779
Anti-mouse CD117	BioLegend	Cat#105815; RRID:AB_493472
Anti-mouse Sca-1	BioLegend	Cat#108107; RRID:AB_313345
Anti-mouse CD16/32	BioLegend	Cat#101317; RRID:AB_2104156
Anti-mouse CD34	Thermo Scientific	Cat#50-0341-80; RRID:AB_10609352
Anti-mouse CD150	BioLegend	Cat#115903; RRID:AB_313682
Anti-mouse CD41	BioLegend	Cat#133903; RRID:AB_2129746
Anti-Ly6G mAB depletion antibody	Bio X Cell	Cat##BE0075-1; RRID:AB_1107721
InVivoMAb rat IgG2a isotype control	Bio X Cell	Cat#BE0089; RRID:AB_1107769
Ultra-LEAF™ Purified anti-mouse CD28 Antibody	Biolegend	Cat#102116; RRID:AB_2810333
Cit-Histone3 antibody	Abcam	Cat#Ab5103; RRID:AB_304752
Ultra-LEAF™ Purified anti-mouse CD3e Antibody	Biolegend	Cat#100340; RRID:AB_2616674
Anti-mouse F4/80	Thermo Scientific	Cat#17-4801-82; RRID:AB_2784648
Chemicals, peptides, and recombinant proteins		
DSS	MP Biomedicals	Cat#0216011080
Tamoxifen	Sigma-Aldrich	Cat#T5648
Recombinant G-CSF	PeproTech	Cat#250-05
Recombinant Mouse IGSF2/CD101 Fc Chimera Protein, CF	R&D Systems	Cat#3368-CD-050
Recombinant Mouse IgG2A Fc Protein, CF	R&D Systems	Cat#4460-MG-100
Critical commercial assays		

REAGENT or RESOURCE	SOURCE	IDENTIFIER
Corn oil	Sigma-Aldrich	Ca#C8267
Red blood cell lysis buffer	Sigma-Aldrich	Cat#R7757
CD8$^+$ T cell isolation kit	Miltenyi Biotech	Cat#130-096-543
Anti-Ly6G MicroBeads UltraPure	Miltenyi Biotec	Cat#130-120-337
DPBS without Calcium and Magnesium	Fisher Scientific	Cat#14-190-250
1X HBSS no Ca Mg phenol red	Thermo Fisher	Cat#14175-103
Fetal Bovine Serum, Qualified, Heat Inactivated	Thermo Scientific	Cat#10438026
Gibco™ RPMI 1640 Medium	Fisher Scientific	Cat#11-875-119
Collagenase type II	Thermo Fisher Scientific	Cat#17-101-015
Collagenase D	Sigma-Aldrich	Cat#11088866001
EDTA, 0.5M SOLUTION, PH 8.0	AmericanBio	Cat#AB00502-01000
DTT	Sigma-Aldrich	Cat#646563
Dispase II	Sigma-Aldrich	Ca#04942078001
DNase I	Sigma-Aldrich	Cat#11284932001
Live-Dead dye	Thermo Scientific	Cat#L34957
Flow cytometry staining buffer	eBioscience	Cat#00-4222-26
Purified Rat Anti-Mouse CD16/CD32 Fc block	BD Bioscience	Cat#553142
CountBright™ Absolute Counting Beads	ThermoFisher	Cat#C36950
SMARTpool: ON-TARGETplus Mouse CD101 siRNA	Horizon Discovery Biosciences	Cat#L-076576-01-0005
P3 Primary Cell 4D-Nucleofector® X Kit	Lonza	Ca#V4XP-3024
RNeasy Plus mini kit	Qiagen	Cat#74134
iScript cDNA synthesis kit	Bio-rad	Cat#1708891
iTaq Universal SYBR Green Supermix	Bio-rad	Cat#1725121
CFSE dye	ThermoFisher	Cat#C34554
DDAO-SE Far-red dye	ThermoFisher	Cat#C34564
H2DCFDA ROS dye	ThermoFisher	Cat#D399
Liberase™ DL	Sigma-Aldrich	Cat#05401160001
4% buffered formalin	Santa Cruz	Cat#sc-281692
Deposited data		
Single cell RNA seq	This manuscript	ProteomeXchange: PXD048613
MS analysis	This manuscript	GEO: GSE255409
Experimental models: Organisms/strains		
Mouse: Wnt5a$^{flox/flox}$	The Jackson Laboratory	Strain #:026626
Mouse: Wnt5b$^{-/-}$	International Mouse Strain Resource	Komp #:14908
Mouse: Rosa26-CreER(T2) mice	The Jackson Laboratory	Strain #:008463
Oligonucleotides		
Primers for PCR and RT-qPCR	Integrated DNA Technologies	listed in the STAR Methods
Software and algorithms		

REAGENT or RESOURCE	SOURCE	IDENTIFIER
GraphPad Prism 9.0	GraphPad Software	https://www.graphpad.com/
ImageJ	National Institutes of Health	https://imagej.net/ij/
FlowJo	FlowJo, LLC	https://www.flowjo.com/